# THE BREAKUP OF FLOCS IN A TURBULENT FLOW FIELD

by

JYH PING HSU

B. S., National Taiwan University, 1977

---

A MASTER'S THESIS

submitted in partial fulfillment of the

requirements for the degree

MASTER OF SCIENCE

Department of Chemical Engineering

KANSAS STATE UNIVERSITY
Manhattan, Kansas

1980

Approved by:

Larry Allen Glasgow
Major Professor

**THIS BOOK IS OF POOR LEGIBILITY DUE TO LIGHT PRINTING THROUGH OUT IT'S ENTIRETY.**

**THIS IS AS RECEIVED FROM THE CUSTOMER.**

TABLE OF CONTENTS

# CHAPTER 1

## INTRODUCTION

The removal of solid impurities in water and wastewater treatment is normally accomplished by sedimentation. Since many of the impurities are too small for gravitational settling, the aggregation process is necessary as a precursor. Deaggregation, a phenomenon which inevitably accompanies the process, will obviously play an important role in the ultimate determination of floc size. Unfortunately, floc breakup is one aspect of the dynamic behavior of coagulating systems that is not well understood.

The most important physical properties of flocs in the water treatment context are size, density, structural type, and strength (or resistance to deaggregation). Size can be observed directly and the apparent density can be determined from measurements of terminal velocity; structural type and strength, on the other hand, are characteristics that are much more difficult to investigate because they are affected by a host of physicochemical parameters including: solution pH and ionic strength, surface characteristics of the colloidal solid, type of coagulant used, and the level of aggregation at which the particular agglomerate was formed.

Several breakup mechanisms have been proposed in the literature and these include: resonant breakup due to vortex shedding, rotation and deformation by viscous shear, bulgy deformation by fluctuations in dynamic pressure, primary particle erosion by shear, collisional fragmentation, and interaction between particles and impeller vortex system.

Of course, not all of these mechanisms are equally probable for a given environment and floc structure; consider the mechanical differences between flocs formed by: particle capture by enmeshment, macromolecular bridging, adsorption and charge neutralization, bioflocculation, and as a subset of each of the above, different levels of aggregation. Widely different structural types cannot be expected to respond identically to imposed stress.

In order to investigate the relationships between floc strength, size and structural type which are needed to elaborate the population balance model, experiments were conducted in a baffled, stirred tank and a two-dimensional free turbulent jet. The latter was chosen as a pertinent flow field since some similarities are evident between the jet flow and the impeller stream in the tank (compare the mean velocity profiles in Figure 6).

This study provided the following information:

1. Direct observation of the deaggregatiom of individual flocs and thus the breakage mode for flocs formed under various conditions;
2. Estimation of the critical levels of stress and dissipation required for aggregate breakup; quantitative determinations of the strength of floc;
3. The relationship between various floc parameters, including strength, density, size, and structural type;
4. A quantitative description of the distribution of daughter particle sizes and number produced;
5. Some evidence supporting the existence of multiple-levels of aggregation.

6. Observation of the particle size and number distribution in batch deaggregation experiments conducted in a baffled stirred flocculator. A rough population balance model was used to describe the deaggregation history. Some preliminary data on the changes in particle size distribution were obtained.

# CHAPTER 2

## FLOW FIELD IN THE TURBULENT JET APPARATUS

### 2.1 APPARATUS

The experimental apparatus is shown schematically in Figure 1. It consists of a polycarbonate observation chamber, a pumping system, and a high-speed electronic stroboscope. The turbulent jet is produced inside the chamber by the horizontal slit with a height of 0.3 cm and a length of 10.2 cm.

### 2.2 EXPERIMENTAL METHOD AND RESULTS

Analyses of the mean flow in two-dimensional turbulent jets have been discussed by White (1974): the development offering best agreement with experimental data was presented by Reichardt (1942) and by Görtler (1942). The time-average velocity distribution is:

$$U_1/U_{max} = \text{sech}^2 \lambda \qquad (1)$$

where

$$\lambda = \sigma x_2/x_1 \qquad (2)$$

and the coordinate system is as shown in Figure 2. The constant $\sigma$ results from the closure scheme used (a scaling relation for eddy viscosity based upon maximum jet velocity and jet width) to eliminate the Reynolds stress; the value found by Reichardt that gave the best agreement with experimental data was 7.67. Some discrepancy exists between the profile and data near the edge of the jet, but Townsend (1949) has suggested that this is a consequence of intermittency.

The characteristics of the turbulent jet were investigated with both pitot tube traverse and photographic flow visualization. In the mean flow

**THIS BOOK CONTAINS NUMEROUS PAGES WITH DIAGRAMS THAT ARE CROOKED COMPARED TO THE REST OF THE INFORMATION ON THE PAGE.**

**THIS IS AS RECEIVED FROM CUSTOMER.**

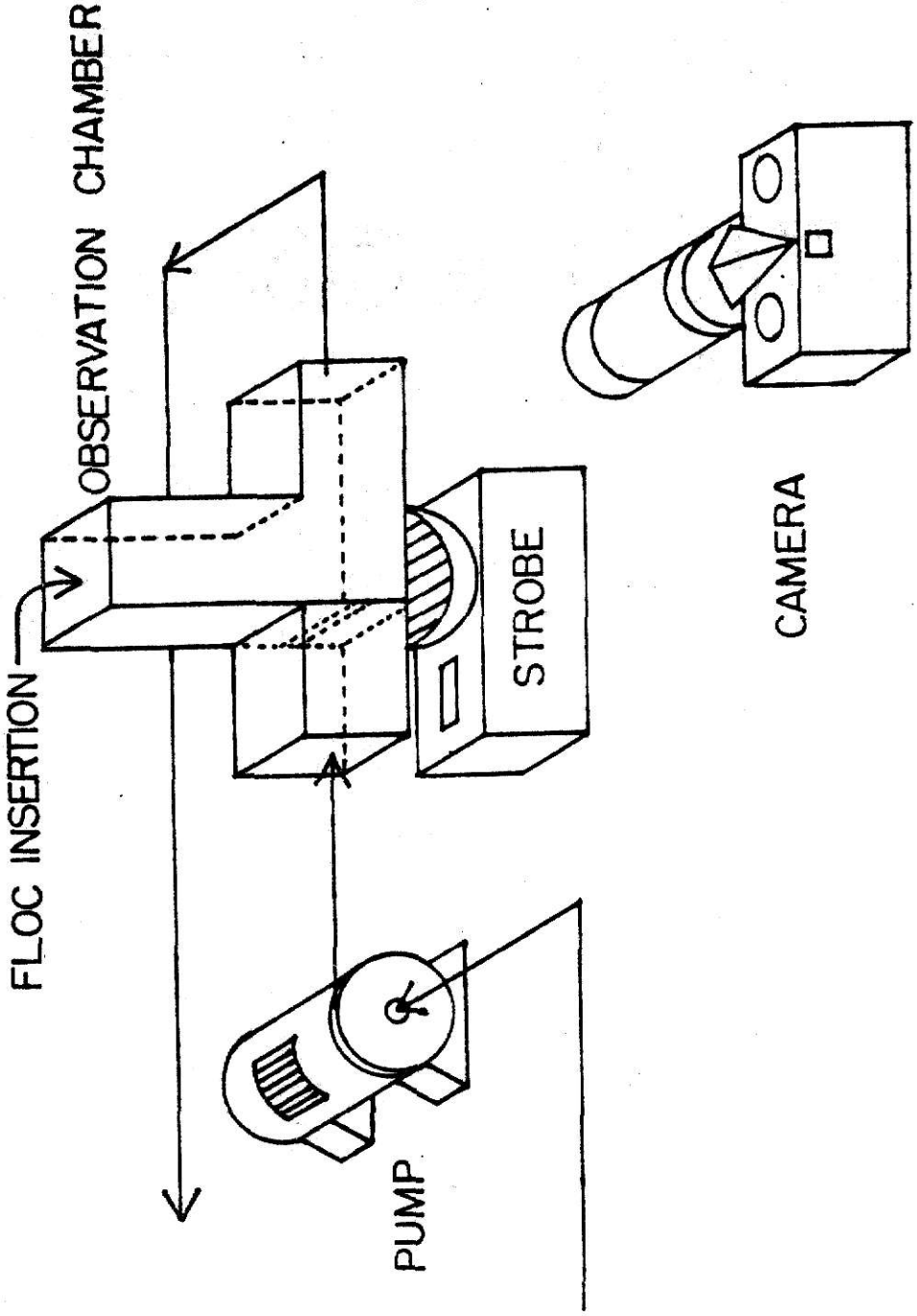


Figure 1. Apparatus Used for Study of Floc Strength.

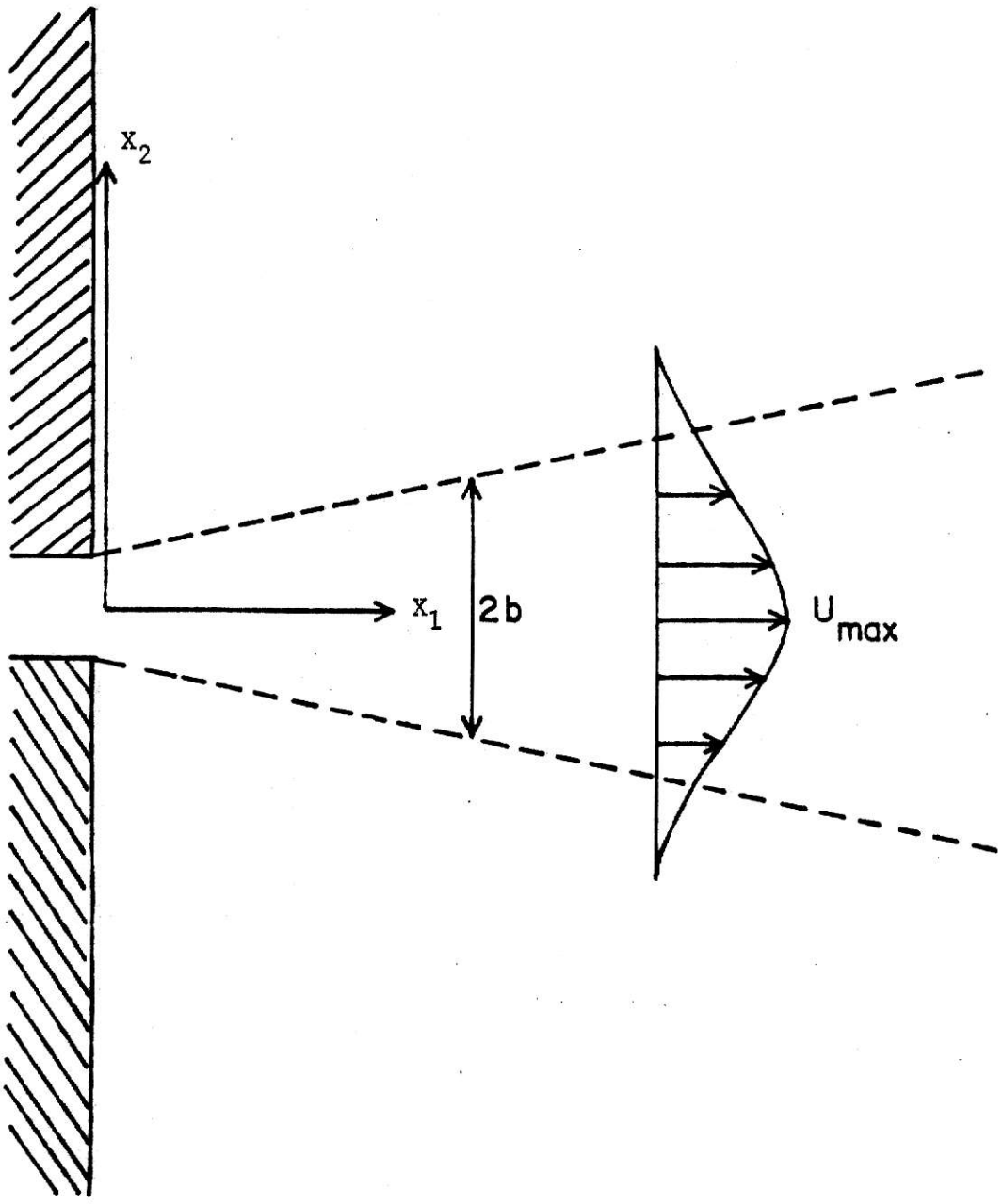


Figure 2. Two—Dimensional Turbulent Free Jet

measurements, a Gould-Statham PM5TC pressure transducer driven at 10 V dc was used in conjunction with a hypodermic-needle pitot tube to determine the total head as a function of vertical position. The inner diameter of the needle tube was 1.09 mm: the inertia of this apparatus was so large that no usable information concerning velocity fluctuations could be obtained. The mean velocity distribution, however, was found to behave much as predicted by the Reichardt and Görtler mixing-length analysis. At a Reynolds number of 7840 (at $x_1 = 0$), and a distance downstream of 1.5 cm, $\sigma$ was found to be approximately 5.1. This is at variance with the value of 7.67 reported in the cited mixing-length analyses but the difference is probably due to the small distance downstream (7.5 h) at which the measurements were made. The mean velocity profiles at different positions are shown in Tables 1 and 2, and in Figure 3.

Quantitative information was obtained from photographic flow visualization by seeding the liquid phase with glass microballoons ( a product of Emerson and Cuming, Inc., Northbrook, Illinois). The microballoons were neutrally buoyant and ranged upwards in size from 10 $\mu$m; due to the inertia effects noted by Hinze (1975), it is probable that the estimates of turbulent fluctuations are conservative. Measurements were made on the jet centerline at values of $x_1$ of 1.52. 1.85, 2.17, and 3.26 cm; the relative intensities at these positions are compiled in Table 3.

The $R_{11}$ correlation coefficient was measured:

$$R_{11}\ (r_1,\ 0,\ 0) = \overline{u_1(x_1)\ u_1(x_1+r_1)}/\overline{u_1^2(x_1)} \qquad (3)$$

and the results are presented in Figure 4. The integral length scale ob-

TABLE 1

MEAN VELOCITY MEASUREMENT AT $X_1$ = 0.5 CM

| Velocities (cm/sec) | Position |
|---|---|
| 221 | center line ($x_2$=0) |
| 120 | -0.1825 cm |
| 66 | -0.3650 cm |
| 56 | -0.5475 cm |
| 56 | -0.7300 cm |
| 167 | +0.1825 cm |
| 56 | +0.3650 cm |
| 44 | +0.5475 cm |
| 44 | +0.7300 cm |

TABLE 2

MEAN VELOCITY MEASUREMENT AT $X_1$ = 1.5 CM

| Velocities (cm/sec) | Position |
|---|---|
| 164 | center line ($x_2$=0) |
| 70 | -0.1825 cm |
| 56 | -0.3625 cm |
| 46 | -0.5475 cm |
| 44 | -0.7300 cm |
| 177 | +0.1825 cm |
| 98 | +0.3625 cm |
| 56 | +0.5475 cm |
| 43 | +0.7300 cm |

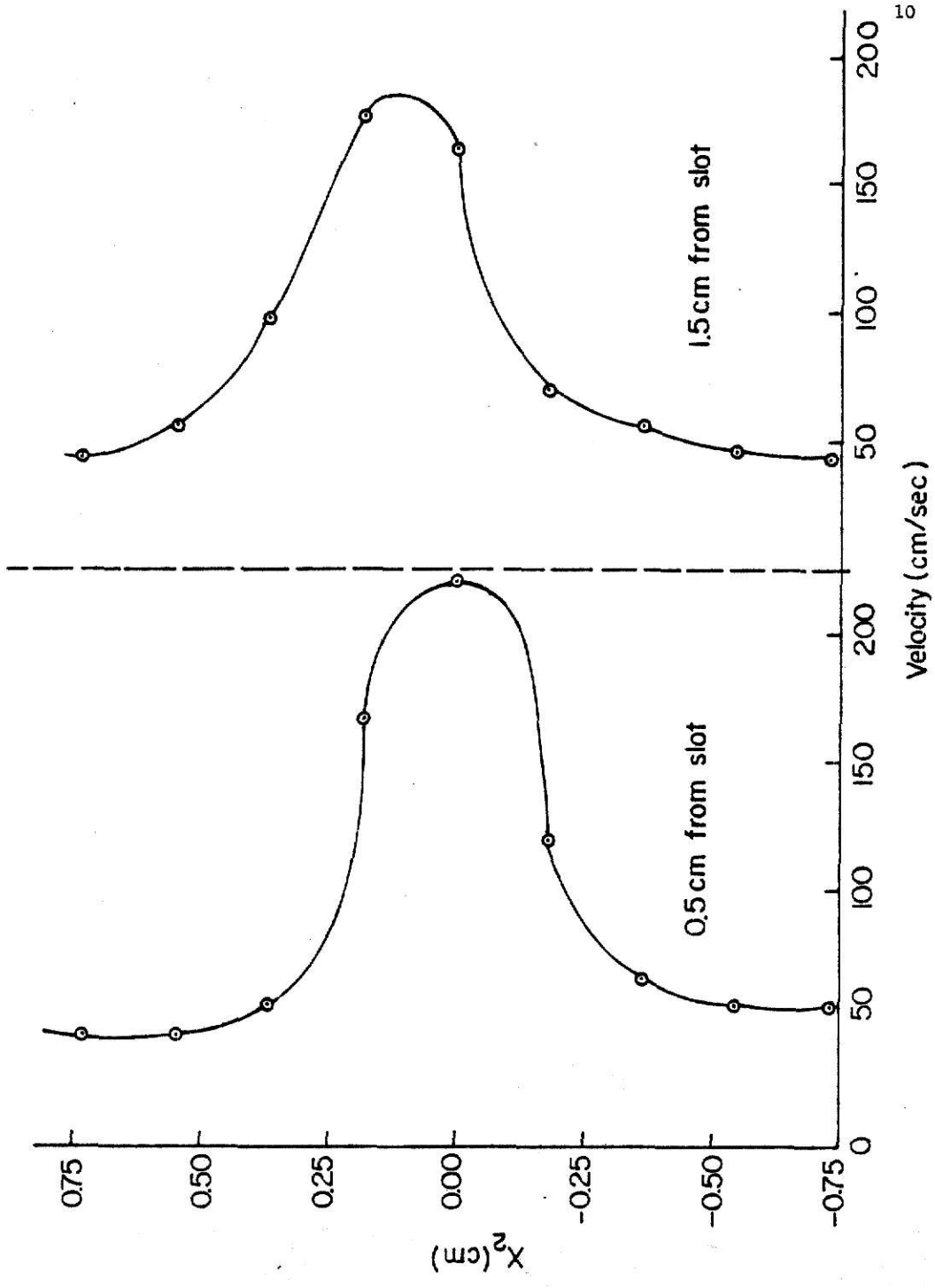


Figure 3. Flow Field of the Turbulent Jet.

TABLE 3

RELATIVE AXIAL INTENSITIES ON JET CENTERLINE AT Re = 3740

| $X_1$ (cm) | $\sqrt{\overline{u_1^2}}/U_1$ | Jet height, h (cm) |
|---|---|---|
| 1.52 | 0.29 | 0.86 |
| 1.85 | 0.32 | 0.96 |
| 2.17 | 0.33 | 1.00 |
| 2.72 | 0.29 | 1.14 |
| 3.26 | 0.34 | 1.26 |

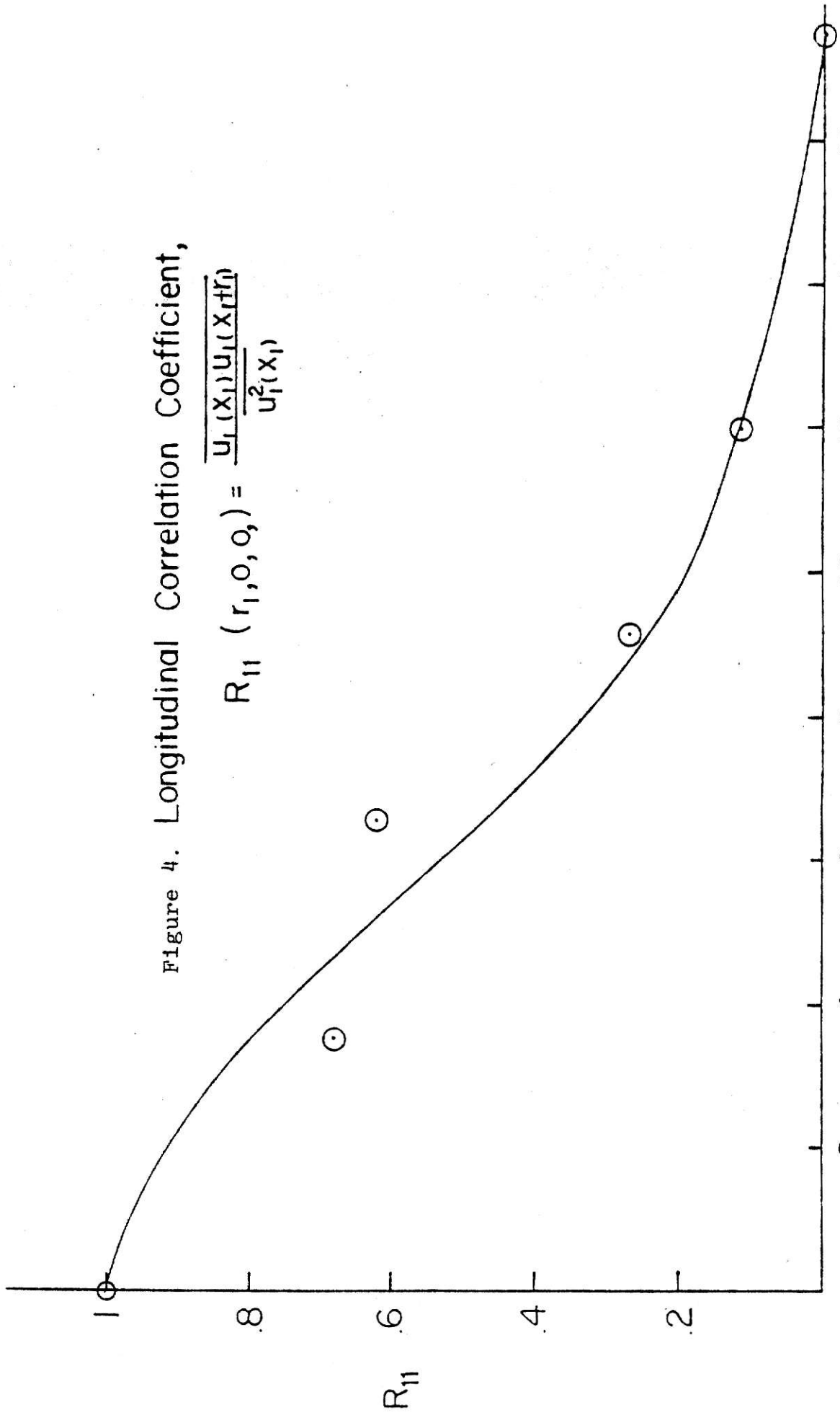
Longitudinal Correlation Coefficient,
$R_{11}(r_1,0,0,) = \frac{\overline{u_1(x_1)u_1(x_1+r_1)}}{\overline{u_1^2(x_1)}}$
$R_{11}$
1
.8
.6
.4
.2
2
4
6
8
10
12
14
16
$r_1$, mm

Figure 4.

THIS BOOK
CONTAINS
NUMEROUS PAGES
WITH THE ORIGINAL
PRINTING BEING
SKEWED
DIFFERENTLY FROM
THE TOP OF THE
PAGE TO THE
BOTTOM.

THIS IS AS RECEIVED
FROM THE
CUSTOMER.

tained by integration of $R_{11}$:

$$\ell = \int_0^\infty R_{11} dr_1 \tag{4}$$

was found to yield $\ell = 6.7$ mm. If this integral scale is used to estimate the dissipation rate from the large-scale dynamics, it is found that $\epsilon \sim 2300$ cm$^2$/sec$^3$. The one dimensional spectrum defined by:

$$F_{11}(\kappa_1) = \frac{1}{2\pi} \int_{-\infty}^{\infty} \overline{u_1(x_1) u_1(x_1+r_1)} \exp(-i\kappa_1 r_1) dr_1 \tag{5}$$

was evaluated from the longitudinal correlation with the assumption that the correlation coefficient is an even function and it is illustrated in Figure 5. It is evident that the spectrum contains no appreciable inertial subrange; this result is expected because of the relatively low Reynolds number of the jet. It may be concluded that there is no range of eddies present in the flow that could be characterized by independence from both mean-flow strain and viscosity.

For the purpose of comparison, the radial velocity profile inside the baffled, stirred tank (see Cutter, 1966) and the mean velocity profile at the center line of the turbulent jet are shown in Figure 6; some similarity is seen to exist between the jet flow and the impeller stream. Note that the tank radius is about 15 cm, the deviation between two velocity profiles at a distance larger than 12.5 cm is due to the radial stream inside the tank approaching the wall; there is no such boundary for the jet. The difference between velocity profiles at distances of 4 to 6 cm is due to differing boundary values for the two flow fields.

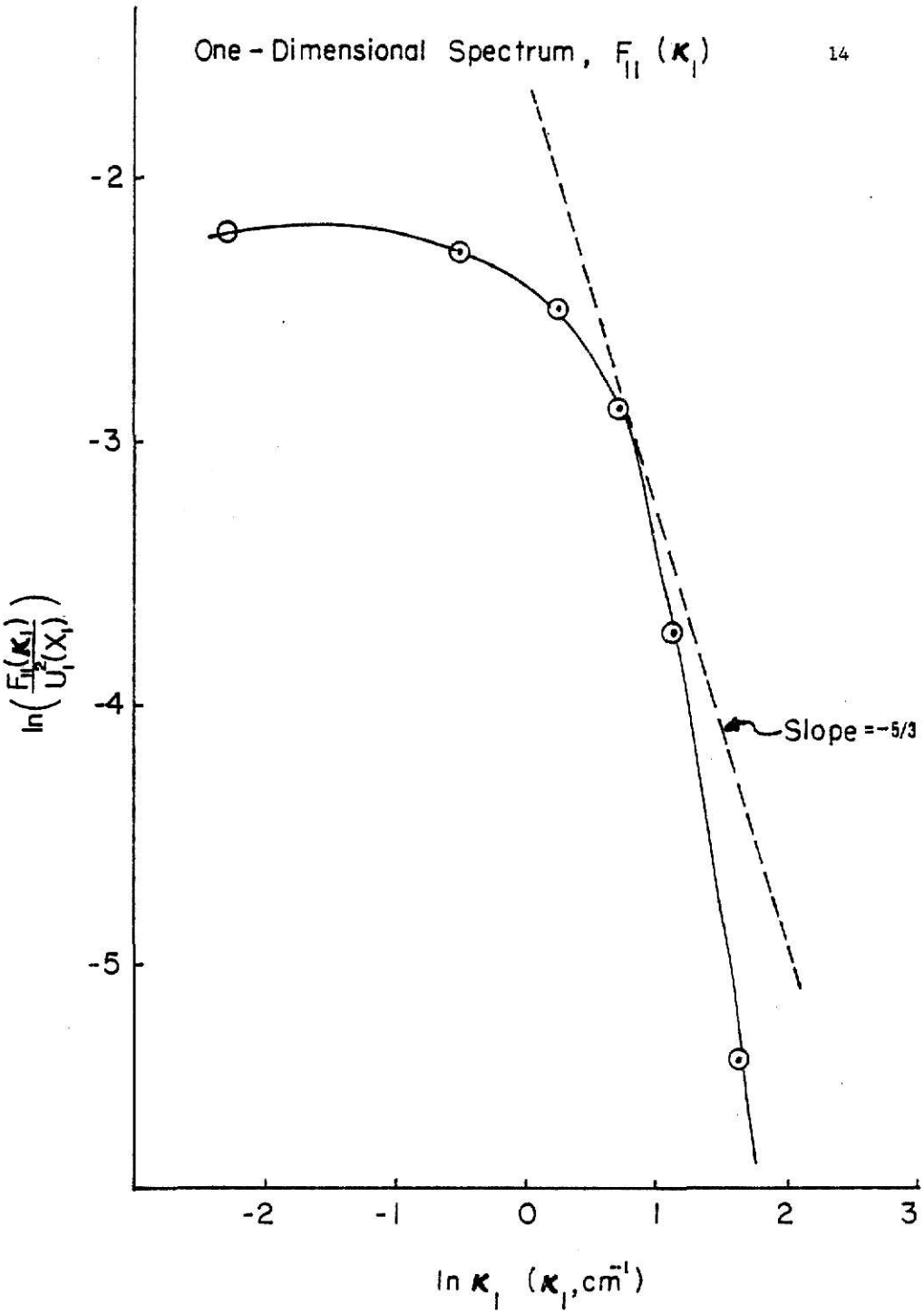
One - Dimensional Spectrum, $F_{11}(\kappa_1)$
$\ln\left(\frac{F_{11}(\kappa_1)}{U_1^2(X_1)}\right)$
-2
-3
-4
-5
Slope = -5/3
-2
-1
0
1
2
3
$\ln \kappa_1$ ($\kappa_1$, $cm^{-1}$)

Figure 5.

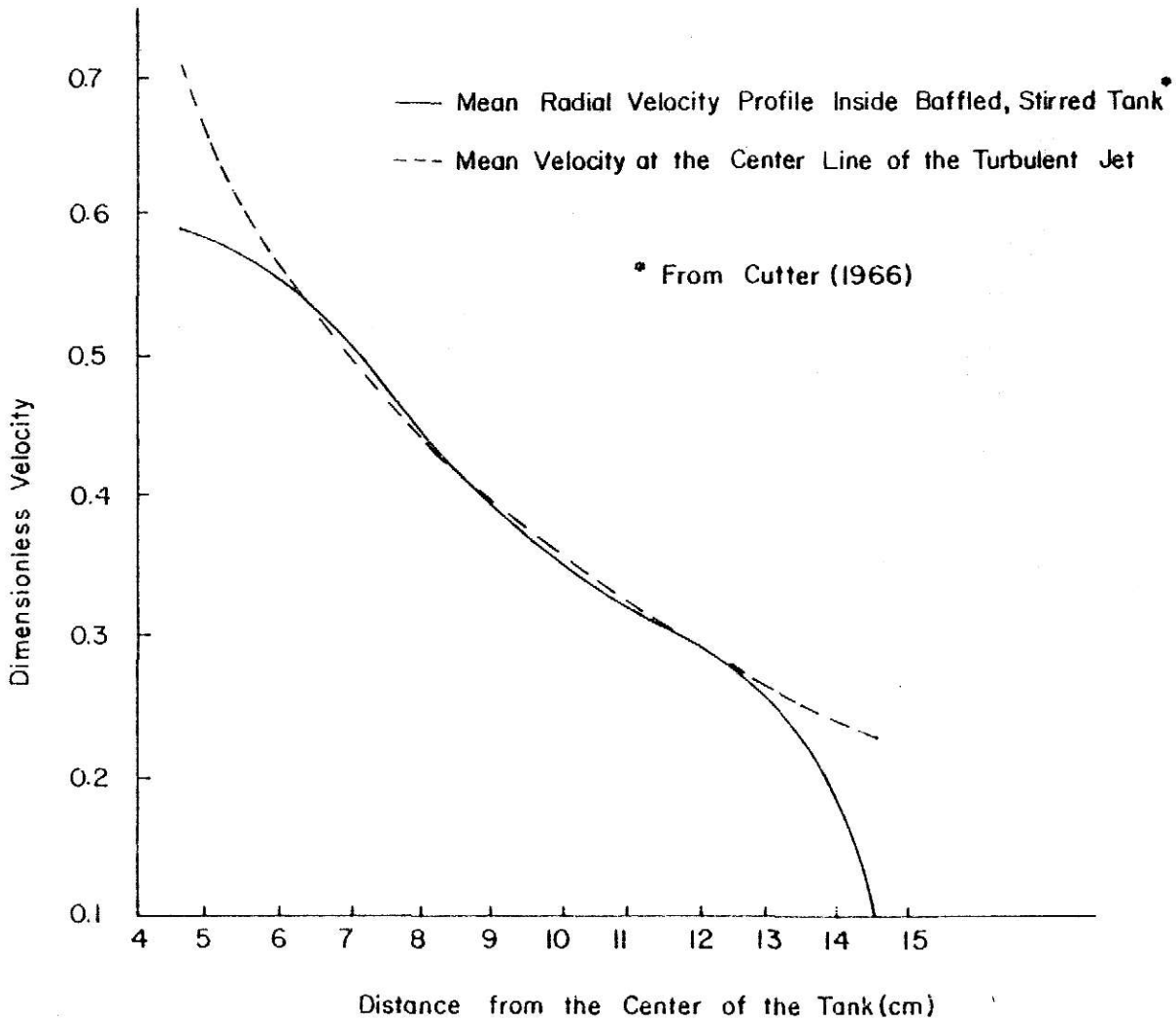


Figure 6. Comparison of Velocity Profiles in Baffled, Stirred Tank and Turbulent Jet.

NOTATION

| | | |
|---|---|---|
| $F_{11}$ | One-dimensional longitudinal spectrum | $cm^3/sec^2$ |
| h | Jet height | cm |
| i | $\sqrt{-1}$ | |
| $\ell$ | Eulerian integral length scale | mm |
| $r_1$ | Spatial separation in $x_1$ - direction | mm |
| $R_{11}$ | Longitudinal correlation coefficient | |
| $u_1$ | Fluctuation velocity in $x_1$ - direction | cm/sec |
| $U_1$ | Mean velocity in $x_1$ - direction | cm/sec |
| $x_1, x_2$ | Coordinate direction and distance | cm |

GREEK LETTERS

| | | |
|---|---|---|
| $\kappa$ | Wave number | $cm^{-1}$ |
| $\lambda$ | Dimensionless position | |
| $\sigma$ | Empirical constant from Reichardt-Görtler velocity distrubution | |
| $\epsilon$ | Dissipation rate | $cm^2/sec^3$ |

## REFERENCES

1. Cutter, L. A., "Flow and turbulence in a stirred tank," Am. Inst. Chem. Engr. J., 12, 35 (1966).

2. Görtler, H., "Berechnung von aufgaben der freien trubelenz auf arund eines neuen naherungsansatzes," ZAMM 22, 244 (1942).

3. Hinze, J. O., "Turbulence," P.145. McGraw-Hill, New York (1975).

4. Reichardt, H., "Gesetzmäbigkeiten der freien turbulenz," VDI-Forschungsh. 414 (1942).

5. Townsend, A. A., "Momentum and energy diffusion in the turbulent wake of a cylinder," Preceedings Royal Society of London, A197,124 (1949).

# CHAPTER 3

## SIZE-DENSITY RELATIONSHIP OF FLOCS

### 3.1 INTRODUCTION

In an effort to obtain more direct evidence concerning the effects of multiple level aggregation, the relationship between floc size and density was examined by measuring the terminal velocity of flocs in a vertical settling chamber. Lagvankar and Gemmell (1968) have presented experimentally determined size-density relationships for flocs formed with $Fe(SO_4)_3$, however, in cases where anionic polyelectrolytes are used as coagulant aids, the different aggregation mechanism involved prevents such results from being compared with Lagvankar and Gemmell's results. Tambo and Watanabe (1979) found that a log-log plot yielded a linear relationship between apparent floc density and size in a study of clay-alum flocs formed under various conditions. A similar logarithmic relationship is found in the study here.

The conformation of polyelectrolyte molecules in a solution undergoing flocculation is significant to the determination of the structure of the floc. A more coiled conformation offers more chances of multiple bonding between macromolecule and colloid particles; the flocs thus formed should have a more compact configuration and should be of a stronger structural type (these aggregates, however, will grow more slowly because of the reduced collision radius).

### 3.2 EXPERIMENTAL PROCEDURE

#### 3.2.1 Kaolin-$Fe^{+3}$ Flocs

Flocs were formed using a multiple-paddle stirrer (a product of Phipps & Bird Inc. Richmond, Virginia) with the following chemical conditions:

kaolin : $4.0 \times 10^{7}$ particles/$cm^{3}$

$NaHCO_3$ : $5.1 \times 10^{-4}$ M

CaO : $5.36 \times 10^{-4}$ M

$FeCl_3$ : $1.85 \times 10^{-4}$ M

Under such conditions the ionic strength is about 0.003 m. Several acidity levels have been investigated to insure production of aggregates characterized by adsorption and charge neutralization on one hand (low pH) and those characterized by particle capture by enmeshment on the other (high pH). Since according to Weber (1972) the isoelectric point of amorphous ferric hydroxide is about pH = 8.0, the pH levels 7.4 and 9.5 were chosen.

Flocs thus formed were introduced into a polycarbonate settling chamber. Multiple flash single frame photographs were taken with Kodak Plus-X Pan film processed at ASA 400 (with a flash rate of 150 fpm). The terminal velocity was deduced from the photographs by measuring the distance traveled by the floc in a fixed time interval.

3.2.2 Kaolin-Polymer-$Fe^{+3}$ Flocs

A commercial polyacrylamide with a molecular weight of 10 to 15 x $10^{6}$ (Betz polymer 1115LP, a product of Betz Laboratories, Inc., Trevose, Pennsylvania) was used as a coagulant aid, with the following initial chemical conditions (the ionic strength is about 0.00295 m):

kaolin : $4.0 \times 10^{7}$ particles/$cm^{3}$

$NaHCO_3$ : $5.1 \times 10^{-4}$ M

CaO : $5.36 \times 10^{-4}$ M

$FeCl_3$ : $1.39 \times 10^{-4}$ M

polymer: 5 ppm

The optimal dosage of coagulant aid was determined by jar test; the dosage which gave the maximum transmittance (or approximate minimum turbidity) was chosen for all further experiments. The degree of transmittance was measured with a Spectronic 600 Spectrophotometer, (product of Bausch & Lomb Co. Rochester, New York) using tungsten light source of a wave length of 560 $\mu$m. The results are shown in Figure 7. It is clear that a polymer concentration of around 4 or 5 ppm gave maximum turbidity reduction.

Two different pH ranges were selected for study, 7.2 and about 10.4- the latter is well in excess of the isoelectric points of edge alumina (~7.8) and edge silica (~2) cited by Birkner and Edzwald (1969). This was done to guarantee appreciable coulombic repulsion between proximate kaolin particles and thereby make interparticle bridge formation requisite to floc growth.

Terminal velocity and floc size were measured photographically as in the case of kaolin-$Fe^{+3}$ flocs.

3.3 TREATMENT OF DATA

The apparent density of floc was calculated by measuring the terminal velocity of individual floc. Since the Reynolds number was beyond the creeping flow range, a generalized relationship between drag coefficient and Reynolds number was used with the assumption that the sphericity of each floc is unity. Figure 8 and 9 show the observed trend for clay-$Fe^{+3}$ flocs formed at pH = 9.5 and pH = 7.4 respectively. In general, as the mean diameter of floc increases, the apparent density decreases.

In the case of kaolin-polymer flocs the relationship between apparent density and floc size at two different pH ranges is shown in Figure 10. Apparent density at a pH of about 10.6 is larger than that at pH = 7.2; this result can be inferred from the viscosity-pH relation (Figure 11). Since at

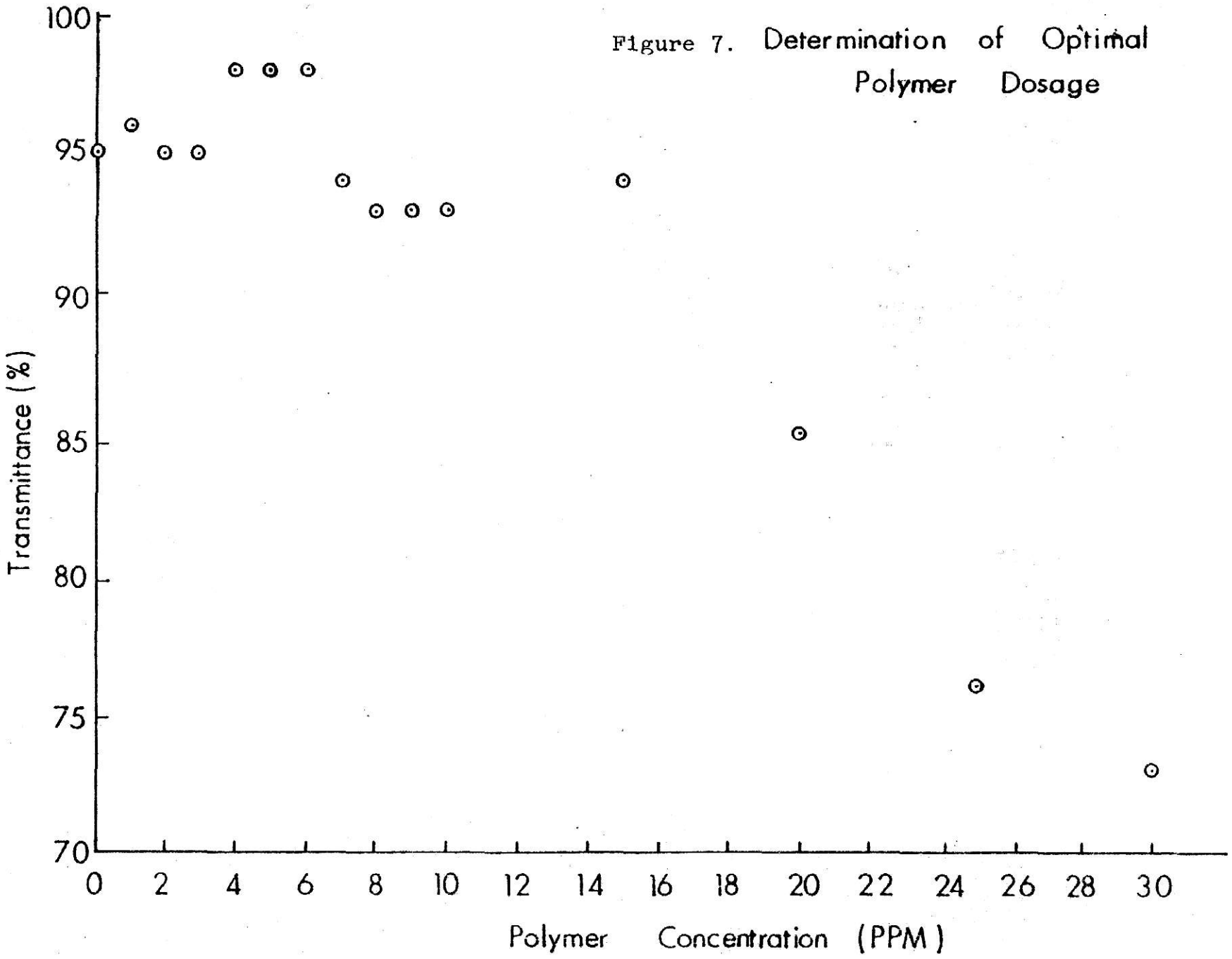


Figure 7. Determination of Optimal Polymer Dosage

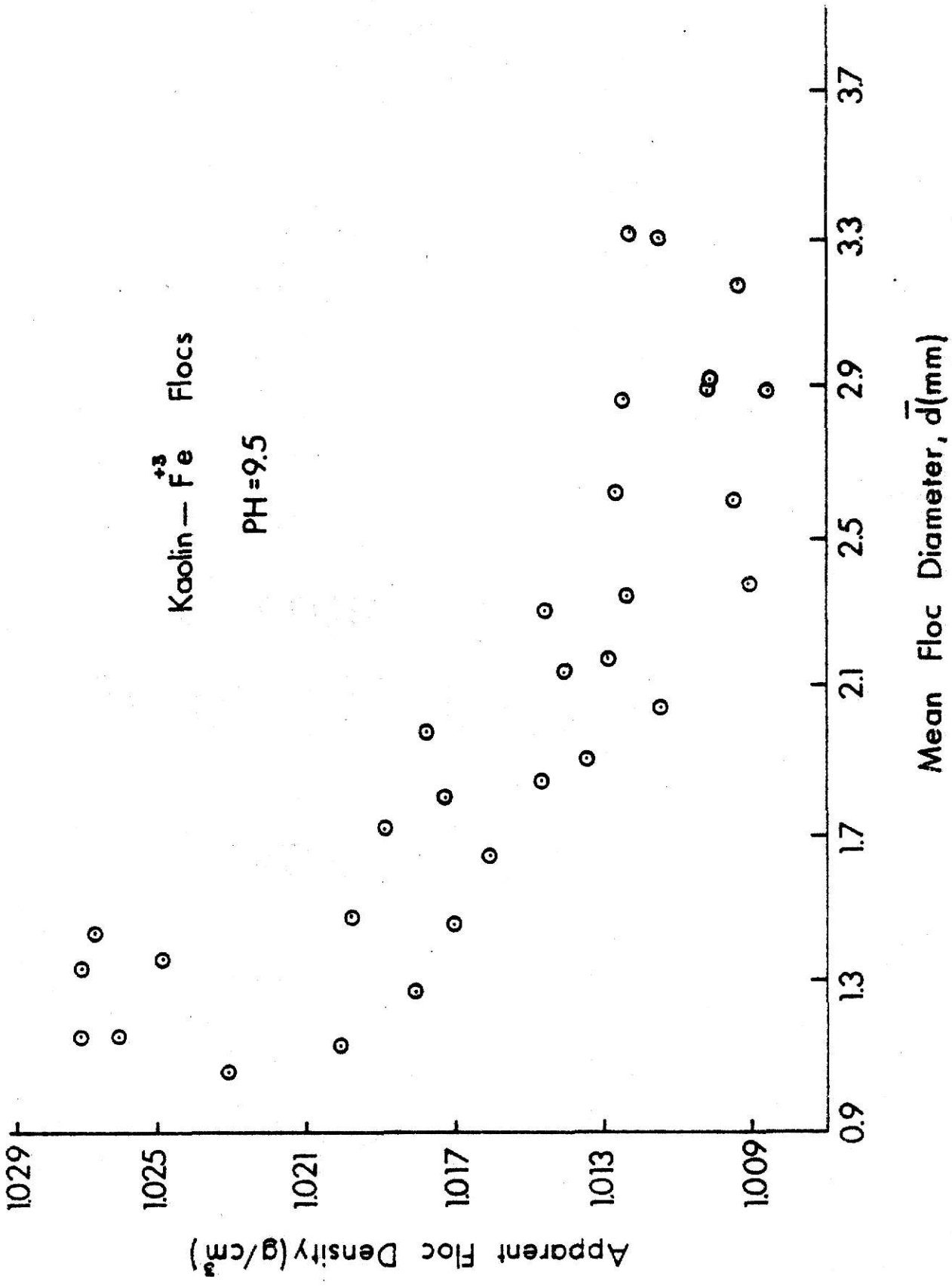
Kaolin — $Fe^{+3}$ Flocs
PH=9.5
Apparent Floc Density (g/cm³)
1.029
1.025
1.021
1.017
1.013
1.009
0.9
1.3
1.7
2.1
2.5
2.9
3.3
3.7
Mean Floc Diameter, $\bar{d}$(mm)

Figure 8.

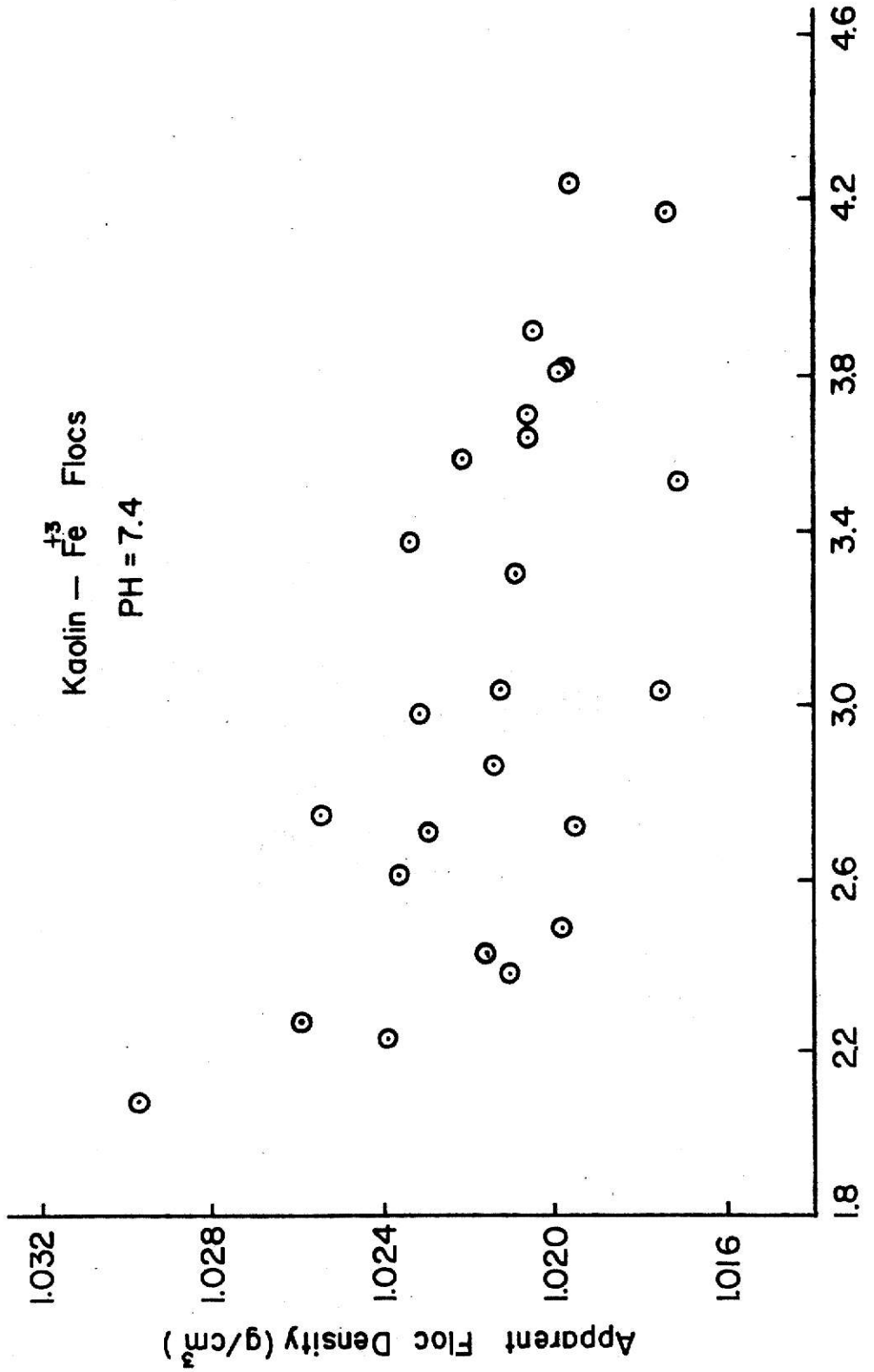
Kaolin — $Fe^{+3}$ Flocs
PH = 7.4
Apparent Floc Density (g/cm³)
1.032
1.028
1.024
1.020
1.016
1.8
2.2
2.6
3.0
3.4
3.8
4.2
4.6
Mean Floc Diameter, $\bar{d}$(mm)

Figure 9.

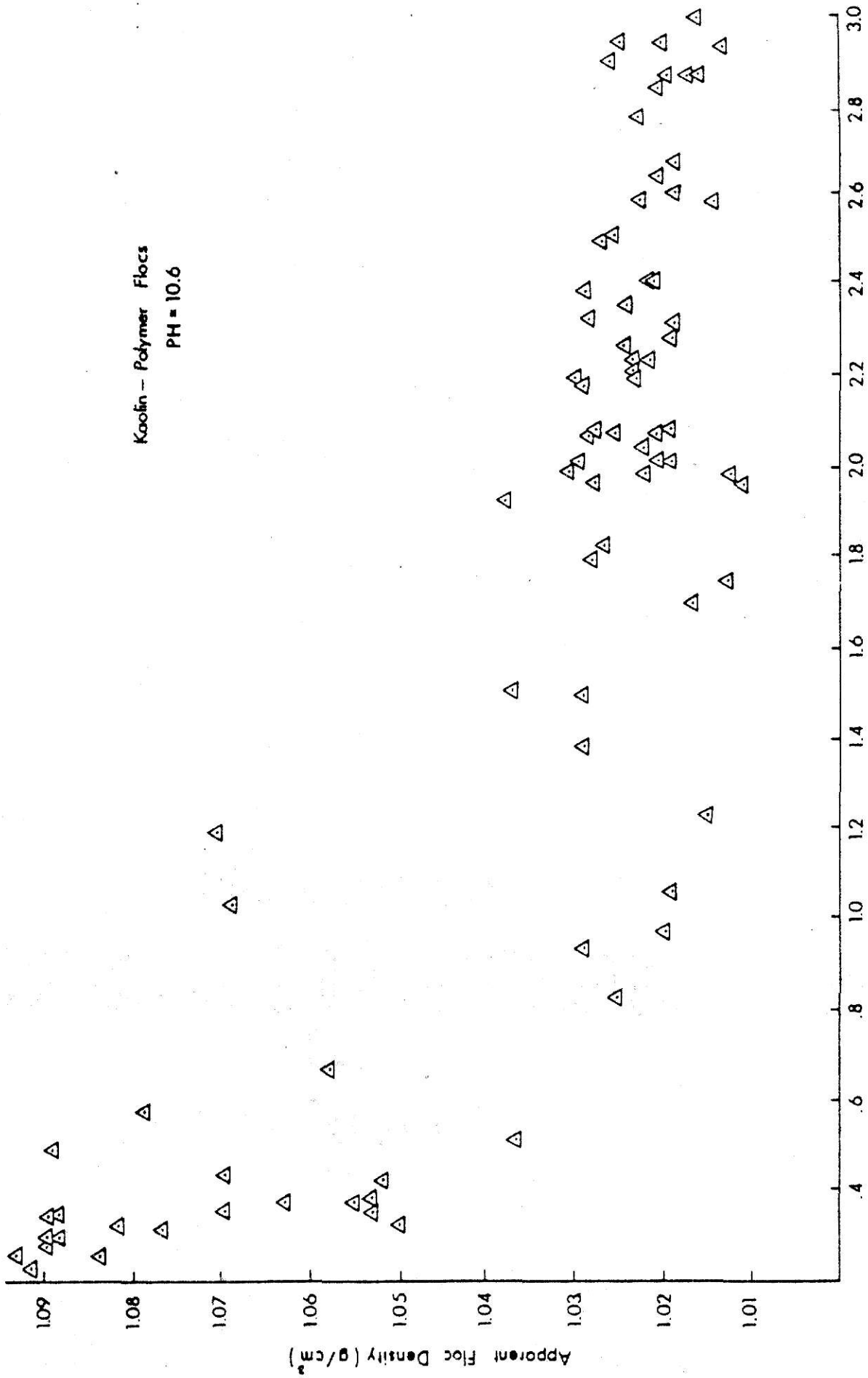
Kaolin – Polymer Flocs
PH = 10.6
Apparent Floc Density (g/cm³)
1.09
1.08
1.07
1.06
1.05
1.04
1.03
1.02
1.01
.4
.6
.8
1.0
1.2
1.4
1.6
1.8
2.0
2.2
2.4
2.6
2.8
3.0
Mean Floc Diameter, d̄ (mm)

Figure 10.

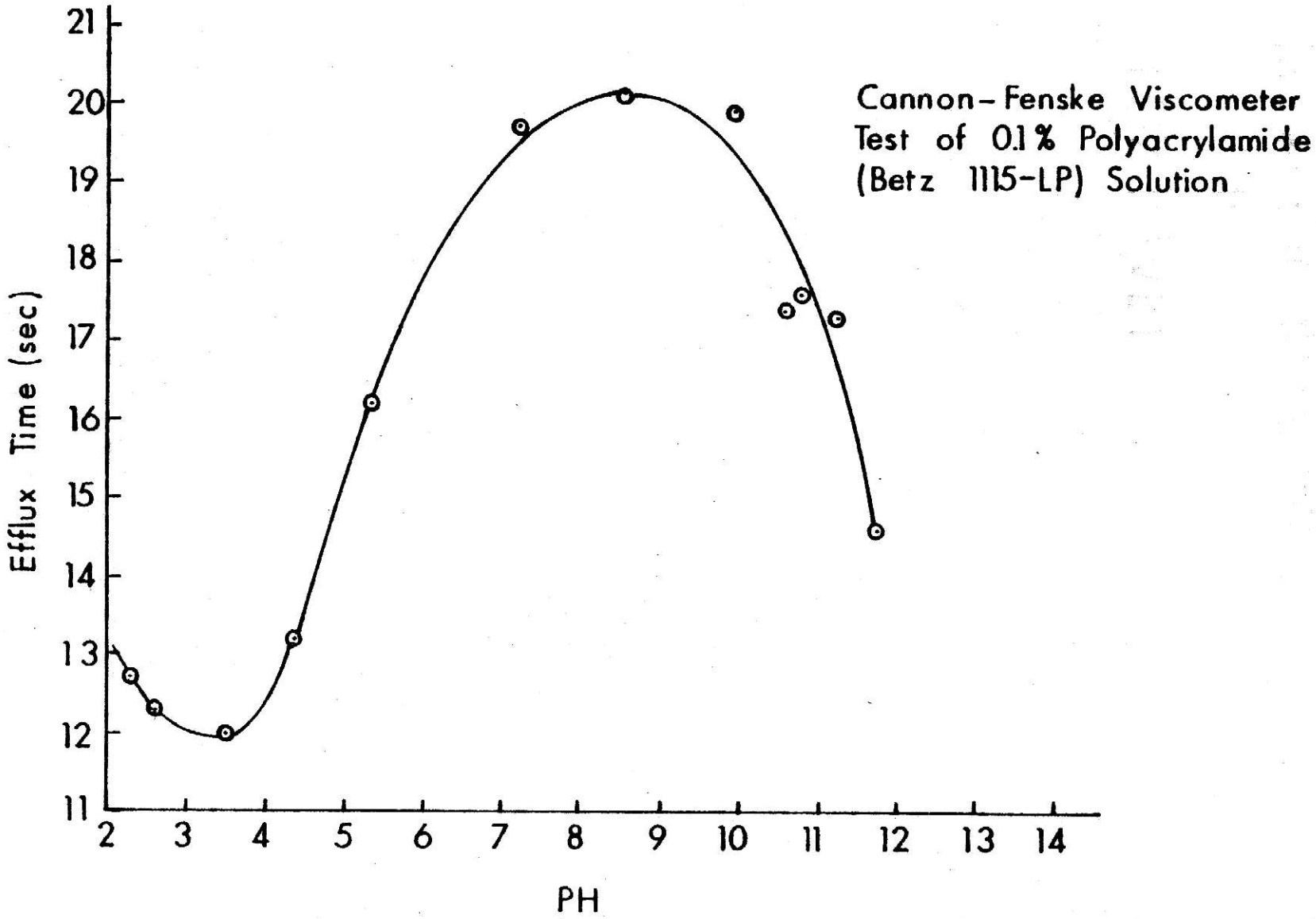
Cannon-Fenske Viscometer
Test of 0.1% Polyacrylamide
(Betz 1115-LP) Solution
Efflux Time (sec)
21
20
19
18
17
16
15
14
13
12
11
2
3
4
5
6
7
8
9
10
11
12
13
14
PH

Figure 11.

pH = 7.2 the polyacrylamide has a more extended conformation (higher viscosity) than at pH = 10.6, a denser structure at pH = 10.6 is anticipated.

NOTATION

| | | |
|---|---|---|
| $\bar{d}$ | Geometric mean aggregate diameter | mm |

## REFERENCES

1. Birkner, F. B..& Edzwald, J. K. "Nonionic polymer flocculation of dilute clay suspension," J. Am. Wat. Wks. Ass., 61, 645 (1969).

2. Lagvankar, A. L. & Gemmell, R. S. "A size-density relationship for flocs," J. Am. Wat. Wks. Ass., 60, 1040 (1968).

3. Tambo, N. & Watanabe, Y., "Physical Characteristics of Flocs-I and II," Water Res., 13, 409 (1979).

4. Walter, J. Weber, JR., "Physicochemical Processes," Wiley-Interscience, New York (1972).

# CHAPTER 4

# STRENGTH OF FLOCS

## 4.1 REVIEW OF PREVIOUS WORK

Floc strength, or resistance to deaggregation, is intimately related to the aggregation process, and is a property which is affected by nearly all of the variables involved in the operation. Although a considerable amount of work has been reported, no direct measurement showing the relation between floc strength and pertinent parameters has been made. A thorough survey of the literature indicates that this is the first quantitative floc strength data available.

For agglomerates formed by interparticle bridging (with macromolecular coagulants), Healy and La Mer (1964) have suggested that strength is related to surface coverage;

$$S \sim \theta ( 1 - \theta ) \qquad (6)$$

where $\theta$ is the fraction of primary particle surface covered by adsorbed polymer. Note that this expression indicates maximum strength when $\theta = 0.5$. An extremely important factor neglected by their analysis, however, is the conformation of the macromolecule at the instant adsorption occurs. It is certain that floc strength in clay polymer systems can be improved by increasing the polymer dosage up to the approach of the point where additional adsorption produces steric or entropic stability. Whether or not this point is coincident with 50% coverage depends largely upon the shape of the sorbent molecules at the interface (in this regard, studies of the pendent-loop configuration are particularly important; see Higuchi,1961,

THIS BOOK CONTAINS NUMEROUS PAGES WITH MULTIPLE PENCIL AND/OR PEN MARKS THROUGHOUT THE TEXT.

THIS IS THE BEST IMAGE AVAILABLE.

and Silberberg, 1962). For anionic polyelectrolytes, elevated pH produces a highly-charged macroion with an extended, rod-like conformation (Oosawa, 1971). This results in a larger effective collision radius and rapid floc growth; the structures, however, are less dense and more susceptible to fragmentation. Lower pH, on the other hand yields a more coiled conformation and an increased likehood of multiple bonding between a single macromolecule and numerous adsorption sites on a single clay particle.

The configurational variation of the polymer used here has been examined. The viscosity of 0.1% polyacrylamide solutions at different pH levels were measured with a Cannon-Fenske viscometer and the results are shown in Figure 11. According to Jirgensons and Straumanis (1962), the viscosity of a polymer solution is larger when the solute polymer has a extended conformation than when it has a more coiled shape; additionally, there exists a minimum in viscosity at the isoelectric point. Figure 11 shows that the isoelectric point of the polymer used is about 3.5.

Hannah, Cohen, and Robeck (1967) studied relative floc strength by drawing aggregates through a 70 $\mu$m orifice; the size of the surviving fragments was thought to be indicative of aggregate strength. The flow rate used in the investigation provided an orifice Reynolds number of about 360. Because size determination was based upon conductivity (actually current interruption), sodium chloride was added to the test solution, assuring that the ionic strength was always in excess of 0.034; this relatively high value results in compression of the ionic atmosphere surrounding the colloidal particles. Kaolin was used as the dispersed phase by Hannah et al., and alum was the coagulant although a polyelectrolyte coagulant aid was used

in one set of experiments; the optimum pH for reduction of the total number of particles was found to be 7.6. This is a reasonable value in view of the isoelectric point data (for kaolinite) cited by Birkner and Edzwald (1969).

Floc strength in polymer-clay systems will also depend upon the level of aggregation at which the particular agglomerate was formed. Michaels and Bolger (1962), Vold (1963), and Lagvankar and Gemmell (1968) have all proposed or advocated multiple-level aggregation. Vold, for example, has suggested three levels; primary colloidal particles, flocs formed entirely by the aggregation of primary particles, and loose aggregates of flocs of the second level.

Another factor affecting the strength of flocs is the distance of approach of interacting colloidal particles during the coagulation process; as the average distance of separation decreases, the possibility of additional bridge formation and the efficacy of van der Waals-London forces are enhanced. A qualitative indicator of the distance of approach of colloidal particles is the "thickness" of the double layer (analogous to the Debye length in the theory of strong electrolytes). van Olphen (1963) gives the "thickness" of the flat double layer, L, as:

$$L = \sqrt{\gamma kT / 4\pi e^2 \Sigma N_i Z_i^2} \qquad (7)$$

Clearly, an increase in the ionic strength of the solution will produce more dense floc structures, containing much less interstitial water. In the systems under study, typical values for L are around 70 Å.

## 4.2 EXPERIMENT AND DATA TREATMENT

Flocs were formed using same apparatus and with same chemical condition as in the study of size-density relationship disscussed in Chapter 3.

When coagulation was complete, individual aggregates were carefully transferred to a polycarbonate observation chamber with a serological pipette and allowed to attain terminal velocity. After settling approximately 30 cm, the floc would encounter a horizontally-directed turbulent jet. The subsequent rapid displacement and fragmentation of the parent aggregate were recorded photographically using an extremely short duration repetitive strobe and a 35 mm camera with Kodak Plus-X Pan film processed at ASA 400. An example of such a record is shown in Figure 12.

The objectives of this work included: direct observation of the deaggregation of individual flocs, estimates of the critical level of stress required for aggregate breakup, quantitative description of the distribution of daughter particle sizes, and relationships between various floc parameters, particularly strength, density, size, and structural type.

The kaolin-$Fe(OH)_3$ flocs selected for the deaggregation experiments ranged in size from about 700 $\mu$m to 3500 $\mu$m. It should be noted that the flash interval was 1/10 second, therefore, periodic disturbances with frequencies much greater than about 1 Hz would not be detected. This is of no real importance, however, as the observed breakup could only be caused by stresses imposed by the mean flow or by integral-scale eddies during the entrainment process. For example, typical critical acceleration levels for 1500 $\mu$m kaolin-$Fe(OH)_3$ flocs formed at an ionic strength of 0.0034 m and a pH of 9.5 were found to be on the order of 80 $cm/sec^2$. The eddy scale required to produce such an acceleration would be many times greater than the parent particle size, say, 1 to 10 cm. Since:

$$a_c \sim u^2/\ell\,, \tag{8}$$

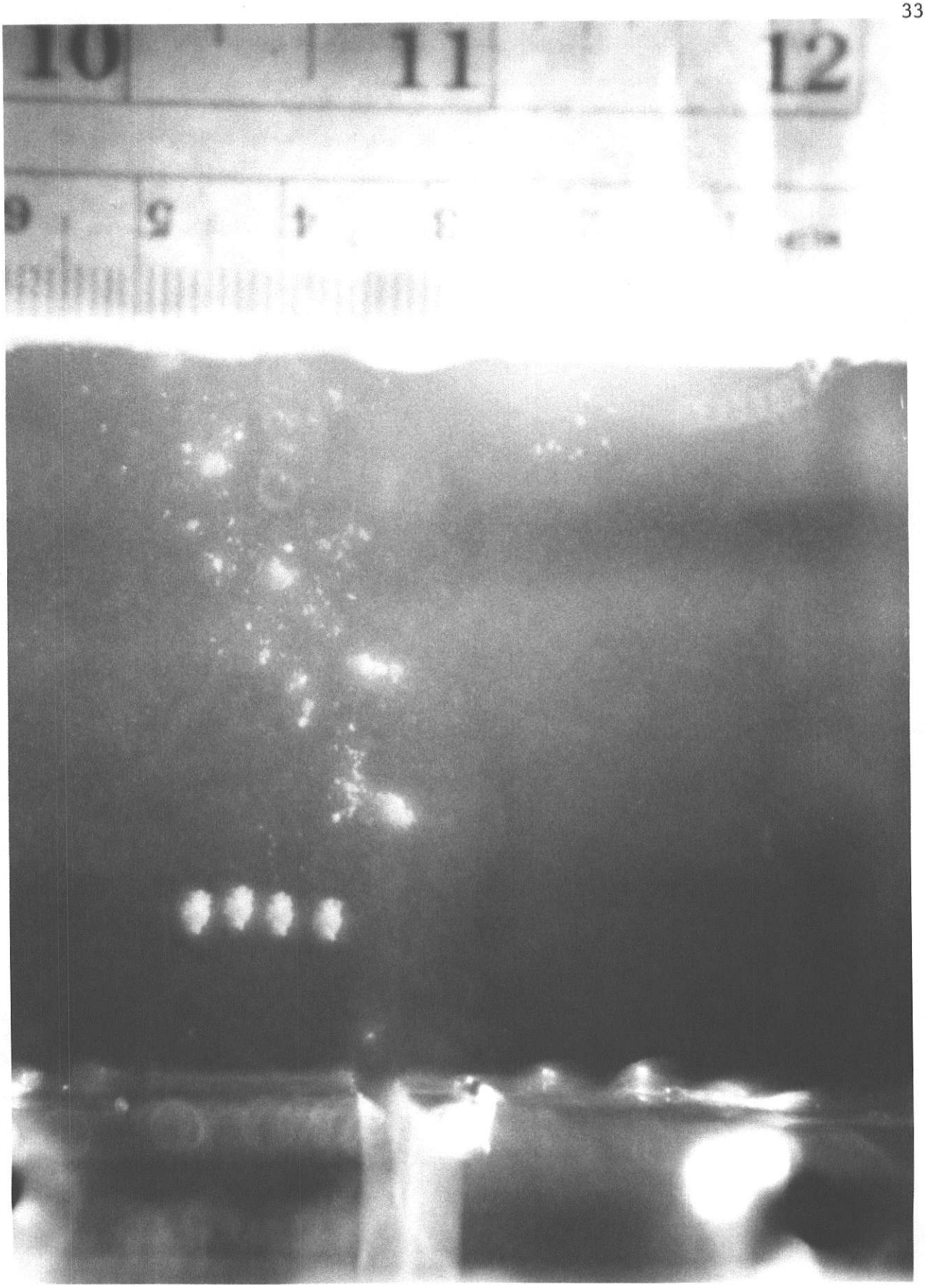


Figure 12. Breakup of Floc in Turbulent Jet.

one may argue that u is on the order of 16 cm/sec. Estimating the critical dissipation rate from the large-scale dynamics,

$$\epsilon \sim u^3/\ell \,, \tag{9}$$

then $\epsilon \sim 1300$ cm$^2$/sec$^3$. For the experimental results under discussion, the average jet velocity, $U_1$ was approximately 20 cm/sec at the slot opening ($x_1 = 0$); evidently, smaller eddies play no significant role in the observed fragmentation.

Critical levels of stress required for aggregate breakup were identified with the aid of the photographic data cited previously. For kaolin-$Fe(OH)_3$ flocs formed at an ionic strength of 0.0034 m and a pH of 9.5, regression analysis of 52 data points yielded the relationship:

$$S = 0.054\ \bar{d}^{\,2.46} \tag{10}$$

where the critical force, S, is in dynes and the mean diameter, $\bar{d}$, is measured in millimeters. The correlation coefficient for this data was found to be 0.94. Kaolin-$Fe(OH)_3$ flocs formed at similar ionic strength but a pH of 7.4 were found to follow a analogous relationship:

$$S = 0.034\ \bar{d}^{2.44} \tag{11}$$

with a correlation coefficient of 0.88.

These two logarithmic regression lines represent data over a range of mean diameters from about 0.8 to 3.5 mm. Observation of the breakup of a few small flocs indicated that the regression lines shown in Figure 13 are not applicable for $\bar{d} \leq 0.5$ mm; the slope in this range is reduced to something on the order of 1.0. It is felt that this discontinuity in

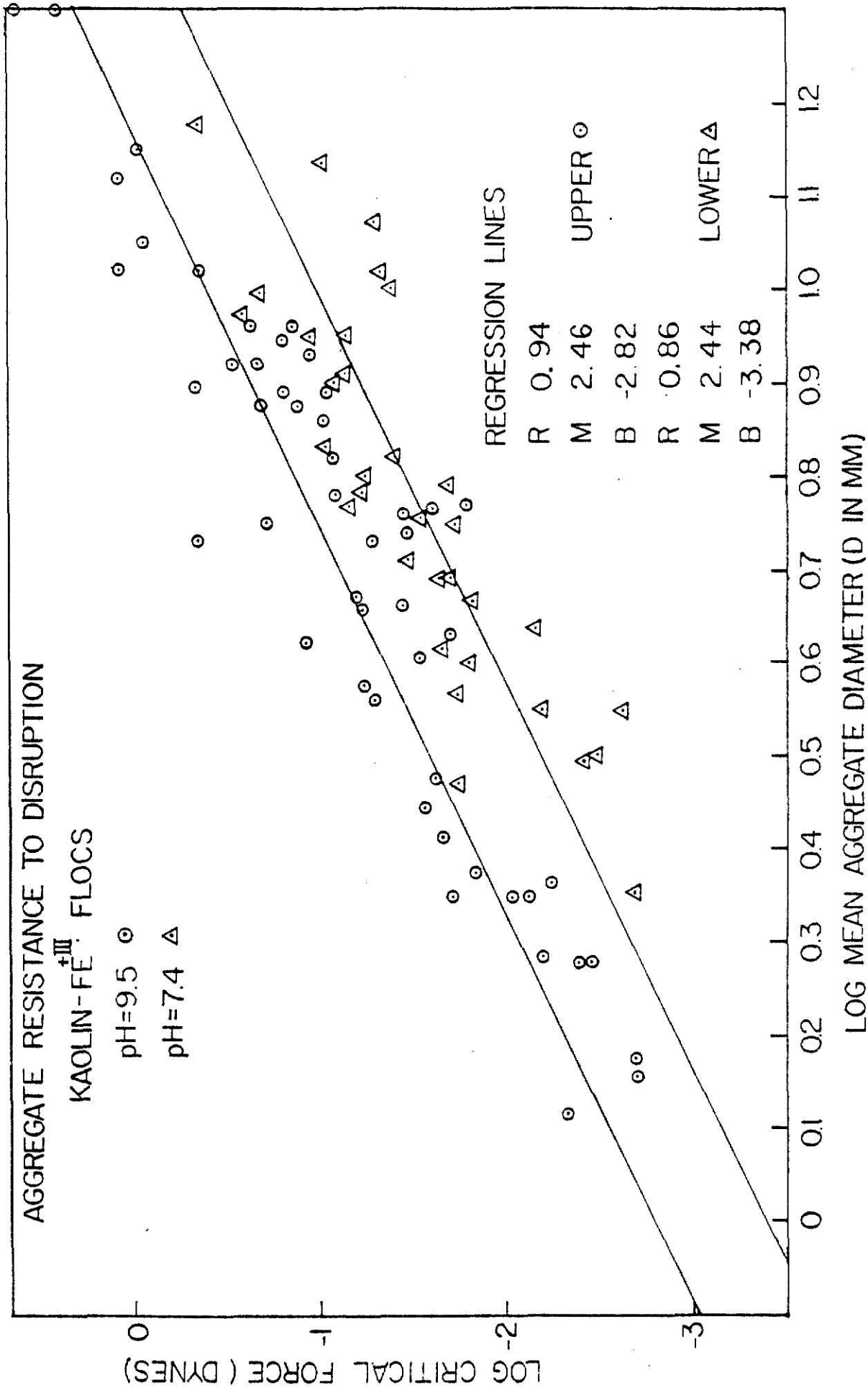
AGGREGATE RESISTANCE TO DISRUPTION
KAOLIN-$Fe^{+III}$ FLOCS
pH=9.5 ⊙
pH=7.4 △
REGRESSION LINES
R 0.94
M 2.46
B -2.82
UPPER ⊙
R 0.86
M 2.44
B -3.38
LOWER △
LOG CRITICAL FORCE ( DYNES)
0
-1
-2
-3
0
0.1
0.2
0.3
0.4
0.5
0.6
0.7
0.8
0.9
1.0
1.1
1.2
LOG MEAN AGGREGATE DIAMETER (D IN MM)

Figure 13.

slope is indicative of the existence of multiple levels of aggregation, i.e., that a change in predominant structural type occurred for the experimental conditions at $\bar{d} \simeq 0.5$ mm.

Daughter-particle sizes and number produced upon fragmentation have been found to be highly variable; it was observed however, that higher Reynolds numbers (higher local dissipation rates) tended generally to produce more fragments. With kaolin-$Fe(OH)_3$ flocs, the breakage mode $\delta$ is certainly not binary: the experiments performed indicate a mode, or number of fragments produced upon breakup, of about 10 to 20. Strictly speaking, $\delta$ can be a function of local energy dissipation, floc size, and structural type. Typically, the daughter particles include one large fragment with a mean diameter of about 70 percent of the parent value and a number of smaller fragments ranging from the threshold of detection through several hundred microns. This behavior suggests the smaller fragments are subunits, flocs of a more compact conformation that when loosely affiliated, form the parent aggregate structure.

In the case of flocs formed by using commercial polyacrylamide as a coagulant aid, the flash interval was reduced to 1/20 second. The same type of simple relationship between critical force and floc diameter was capable of data representation, namely:

$$\ln S = m \ln \bar{d} + b \qquad (12)$$

Two defferent pH levels were investigated, but with similar ionic strength as before. Regression analysis of the data points yielded (Figure 14):

$$S = 0.110\, \bar{d}^{2.47} \qquad (13)$$

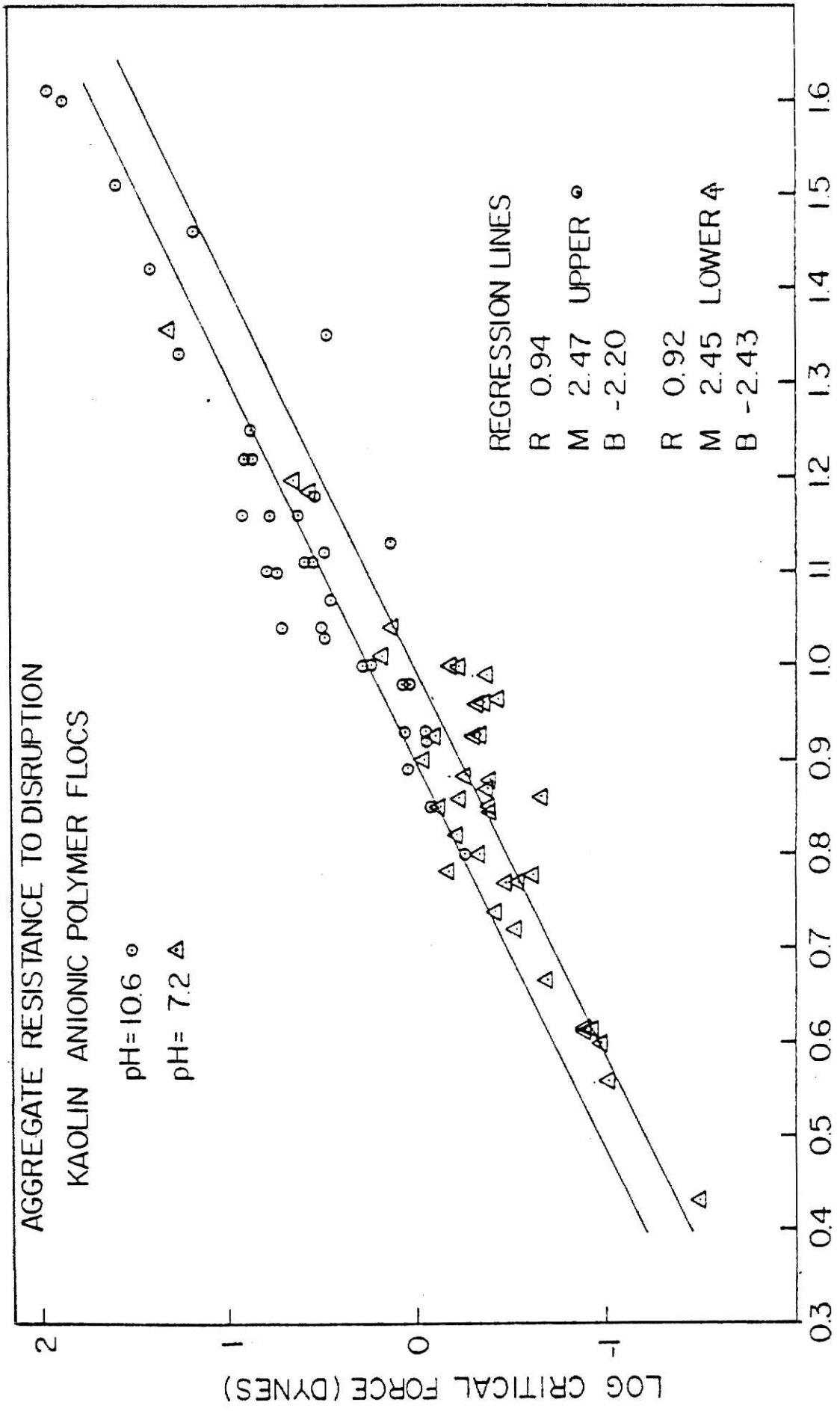
AGGREGATE RESISTANCE TO DISRUPTION
KAOLIN ANIONIC POLYMER FLOCS
pH=10.6 o
pH= 7.2 Δ
REGRESSION LINES
R 0.94
M 2.47 UPPER o
B -2.20
R 0.92
M 2.45 LOWER Δ
B -2.43
LOG CRITICAL FORCE (DYNES)
LOG MEAN AGGREGATE DIAMETER ( D IN MM )
2
1
0
-1
0.3
0.4
0.5
0.6
0.7
0.8
0.9
1.0
1.1
1.2
1.3
1.4
1.5
1.6

Figure 14.

with correlation coefficient 0.94 for a pH of 10.6 and

$$S = 0.008\ \bar{d}^{2.45} \qquad (14)$$

with correlation coefficient 0.92 for a pH of 7.2. The results show flocs formed by using a high-molecular weight polyacrylamide coagulant-aid are more than twice as strong as those formed by using an $Fe^{+3}$ acid-salt alone. The critical force requirement is marginally smaller for lower pH. This phenomenon can be explained by examining the relationship between viscosity of polyacrylamide and pH (Figure 11). At pH = 7.2 the polyelectrolyte possesses a more extended rod-like conformation than at pH = 10.6, thus a weaker linkage between macromolecule and colloidal particle is expected.

Average and maximum floc sizes are larger with the polyacrylamide than with $Fe^{+3}$ alone as anticipated. Again, no systematic behavior was observed for daughter particle sizes and/or number produced. The breakup mechanism appears to be similar to the kaolin-$Fe(OH)_3$ system, a large-scale fragmentation occurring in response to stresses imposed by the mean flow or integral-scale eddies. The daughter particles are, as before, more compact structures formed at a lower level of aggregation.

NOTATION

| | | |
|---|---|---|
| $a_c$ | Critical eddy accleration | $cm/sec^2$ |
| $\bar{d}$ | Geometric mean aggregate diameter | mm |
| e | Constant electronic charge | e.s.u. |
| k | Boltzmann's constant | erg/molecule.K |
| $\ell$ | Eulerian integral length scale | mm |
| L | Thickness of double layer | cm |
| $N_i$ | Number of ions of species i per unit volume | |
| S | Critical forces required for deaggregation | dynes |
| T | Absolute temperature | degree Kelvin |
| u | Fluctuating velocity | cm/sec |
| $Z_i$ | Charge of ion i | |

GREEK LETTERS

| | | |
|---|---|---|
| $\gamma$ | Dielectric constant of fluid medium | |
| $\epsilon$ | Dissipation rate | $cm^2/sec^3$ |
| $\theta$ | Fraction of primary particle surface covered by adsorbed polymer | |
| $\delta$ | Number of daughter particles produced by breakage incident | |

REFERENCES

1. Birkner, F. B. & Edzwald, J. K. "Nonionic polymer flocculation of dilute clay suspension," J. Am. Wat. Wks. Ass., 61, 645, (1969).

2. Hannah, S A., Cohen, J. M., & Robeck, G G., "Measurement of floc strength by particle counting," J. Am. Wat. Wks. Ass., 59, 843 (1967).

3. Healy, T. W. & La Mer, V. K., "The energetics of flocculation and redispersion by polymers," J. Colloid Sci., 19, 323 (1964)

4. Higuchi, W. I., "Effects of short range surface-segment forces on the configuration of an adsorbed flexible chain polymer," J. Phys. Chem., 65, 487 (1961).

5. Jirgensons, B. & Straumanis, M. E., "A Short Textbook of Colloid Chemistry," Macmillan, New York (1962).

6. Lagvankar, A. L. & Gemmell. R. S., "A size-density relationship for flocs," J. Am. Wat. Wks. Ass., 60, 1040 (1968)

7. Michaels, A. S. & Bolger, J. C., "The plastic flow behavior of flocculated kaolin suspensions," I & EC Fundamentals., 1, 153 (1962).

8. Ooswa, F , "Polyelectrolytes," P. 139., Marcel Dekker, New York (1971).

9. Silberberg, A., "The adsorption of flexible macromolecules. Part I. The isolated macromolecule at a plane interface, "J. Phys. Chem., 66, 1872 (1962).

10. van Olphen, H , "An Introduction to clay colloid Chemistry," Interscience, New York (1963).

11. Vold, M. J., "Computer simulation of floc formation in a colloidal suspension," J. Colloid Sci., 18, 684 (1963).

# CHAPTER 5

# FLOC BREAKUP

## 5.1 INTRODUCTION

The mechanism of floc breakup has been studied for many years and a number of conflicting theories regarding the breakup of flocs in turbulent flow fields have been proposed. This diversity of opinion stems partly from lack of direct experimental evidence showing the mode of breakup for individual aggregates in well-characterized turbulent fields. Historically, proposed breakup mechanisms have been based on either of two types of systems: liquid-liquid dispersions (emulsions) and solid dispersions in liquid phase (sols). Some similarity in behavior is observed between the liquid and solid dispersed phase in both cases, yet the mechanism causing the breakage of the dispersed phase is entirely determined by the characteristics of the media, the interactions between them, and the flow field.

## 5.2 BREAKAGE MECHANISM

### 5.2.1 Resonant Breakup:

This mechanism has been suggested by Gunn (1949), Hu and Kintner (1955), and Elzinga and Banchero (1961) in the context of droplet breakup in emulsification processes. Thomas (1964), however, points out that no direct analog of surface tension exists in the case of flocs where particle-particle interactions tend to oppose fragmentation but do not promote vortex-induced oscillation. A possible exception to Thomas's observation might be the case of flocs formed by macromolecular bridging; for these aggregates, the flexible linkages between adjacent particles produce a structure that is surprisingly resilient when subjected to monor defor-

mation. An oscillatory response to periodic disturbance is easily demonstrable in this case.

5.2.2 Deformation and Rupture by Viscous Shear:

According to Hinze (1955) in his discussion of droplet splitting in dispersion processes, a requirement for rupture by viscous shear is that the droplet be small with respect to the Komogorov microscale, $\eta$, where

$$\eta = (\epsilon / \nu^3)^{-1/4} \qquad (15)$$

Generally, the size of large flocs considerably exceeds $\eta$ and thus massive splitting by viscous shear has historically been discounted.

5.2.3 Dynamic Pressure Deformation:

Thomas (1964) advocates bulgy deformation and rupture resulting from random velocity fluctuations as the most plausible mechanism for floc disintegration. The reasoning behind such a hypothesis is due to A. N. Kolmogorov and is summarized by Levich (1962).

Thomas offers the simple dynamic equation:

$$\frac{dN_A}{dt} = \beta N_B - K N_A^2 \qquad (16)$$

where K is the collisional rate constant for reaggregation and $\beta$ is the rate of floc rupture. $\beta$ is described as being comparable to the frequency of occurrence of eddies whose characteristic velocities exceed a threshold value proportional to the square-root of the floc yield stress. Equation (16) is obviously oversimplified since the breakup of floc of size B is not requisite for production of daughter particles of size A, and the disappearance of flocs of size A is not uniquely due to collisions between flocs of

that size.

5.2.4 Particle Erosion by Shear:

This mechanism, advanced by Healy and La Mer (1964), Argaman and Kaufman (1970), and Parker, Kaufman, and Jenkins (1972), envisions a deaggregation process that proceeds through the removal of individual primary particles rather than the massive splitting and rupture envisioned by analogy to theories of emulsification. This is a particularly attractive hypothesis at high Reynolds numbers, because the eddy scales that impart maximum stress upon the floc structure lie primarily in the inertial subrange of the three-dimensional spectrum of turbulent energy. In this range, energy is distributed by wave number according to the familiar -5/3 power law:

$$E(\kappa) = \alpha\epsilon^{2/3}\ \kappa^{-5/3} \qquad (17)$$

Unfortunately, recent experimental data presented by Glasgow and Luecke (1980) show that primary particle erosion plays a very minor role in the disintegration of clay-polymer flocs. It now seems probable that the mechanism put forward by Kaufman et al. could be valid only for very specific floc structures, for example, those characterized by an absence of both interparticle linkages and coulombic repulsion between neighbors; that is, van der Waal's force is the only contributor to the pair potential.

5.2.5 Collisional Fragmentation:

Ham and Christman (1969) were the first to suggest that floc-floc collisions could produce aggregate breakup and they offered some limited data in support of their hypothesis. Glasgow and Luecke (1980), however, were unable to verify the existence of a collisional disintegration mechanism in a more extensive study of the deaggregation of clay-anionic polymer flocs. It is likely that such a mechanism would be confined to collisions

between very large flocs formed at an upper level of aggregation; since such collisions are infrequent, the rate of fragment production would be small.

5.2.6 Impeller Vortex Breakup

Ali, Yuan, and Tatterson (1979) have studied the dispersion of oil in water using high-speed stereoscopic photography. They found that the trailing vortex systems (shed from the impeller blades) caused the elongation and rupture of parent drops; little dispersion occurred outside the vortex systems. Ali et al. have subdivided the breakup process into three classifications, mean shear, transition, and turbulent comminution. The turbulent comminution mechanism is characterized by the interaction of the dispersed phase with the fine-scale structure of the turbulence; this interaction was generally found to occur in the impeller stream at high agitator speeds and to produce small daughter droplets.

5.3 RESULTS

An example showing the breakup of a floc is shown in Figure 12. The photographic record clearly shows that the breakup mechanism entails massive splitting; primary particles erosion did not contribute significantly to parent particle size reduction. The photographs also show that disintegration was generally preceded by counterclockwise rotation (with the jet moving from left to right in Figure 12) and by elongation parallel to the axis of the two-dimensional plane jet. Similar photographic data was obtained for particles ranging in size from 1.1 to 5.0 mm. The range of jet Reynolds numbers used in this portion of the investigation was 1800 to 3800; these values correspond very roughly to centerline dissipation rates, $\epsilon$, of 1000 to 2000 $cm^2/sec^3$. The mean number of daughter particles produced upon fragmentation

was found to be about 10 to 20 for all experimental conditions studied.

NOTATION

| | | |
|---|---|---|
| $E(\kappa)$ | Three-dimensional wave number spectrum | $cm^3/sec^2$ |
| K | Collision rate constant | $cm^3/sec$ |
| $N_A, N_B$ | Number density of particles of type A, B | $cm^{-3}$ |

GREEK LETTERS

| | | |
|---|---|---|
| $\alpha$ | Spectrum constant for inertial subrange | |
| $\beta$ | Deaggregation rate constant | $sec^{-1}$ |
| $\epsilon$ | Dissipation rate | $cm^2/sec^3$ |
| $\eta$ | Kolmogorov microscale | cm |
| $\kappa$ | Wave number | $cm^{-1}$ |
| $\nu$ | Kinematic viscosity | $cm^2/sec$ |

REFERENCES

1. Ali, A. M., Yuan, H. S., & Tatterson, G. B , "Liquid-liquid dispersion mechanisms in agitated vessels," Submitted to Chem. Comm. (1979)

2. Argaman, Y. & Edzwald, J. K., "Turbulence and flocculation," J. Sanit. Engng. Div. Proc. Am. Soc. Civ. Engrs., 96 (SA2), 223 (1970).

3. Elzinga, E. R. & Banchero, J. T., "Some observations on the mechanics of drops in liquid-liquid systems," Am. Inst. Chem. Engrs., J. 7, 394 (1961).

4. Glasgow, L. A. & Luecke, R. H., "Mechanisms of deaggregation for clay-polymer flocs in turbulent systems," Ind. Engng. Chem. Fund., 19, 148 (1980)

5. Gunn, R. J., "Mechanical resonance in freely falling raindrops," J. Geophys. Res., 54, 383 (1949).

6. Ham. R. K. & Christman, R. F., "Agglomerate size changes in coagulation," J. Sanit. Engng. Div. Proc. Am. Soc. Civ. Engrs., 95 (SA3), 481 (1969).

7. Healy, T. W. & La Mer, V. K., "The energetics of flocculation and redispersion by polymers," J. Colloid Sci., 19, 323 (1964).

8. Hinze, J. O., "Fundamentals of the hydrodynamic mechanism of splitting in dispersion processes," Am. Inst. Chem. Engrs. J., 1, 289 (1955).

9. Hu, S. & Kinter, R. C., "The fall of single drops through water," Am. Inst. Chem. Engrs. J., 1, 42 (1955).

10. Levich, V. G., "Physicochemical Hydrodynamics," P.457. Prentice-Hall Englewood Cliffs, N. J. (1962).

11. Parker, D. S., Kaufman, W. J., & Jenkins, D. J., "Floc breakup in turbulent flocculation processes," J. Sanit. Engng. Div. Proc. Am. Soc. Div. Engr., 98 (SA1), 79 (1972)

12. Thomas, D G., "Turbulent disruption of flocs in small particle size suspensions," Am. Inst. Chem. Engrs. J., 10, 517 (1964).

# CHAPTER 6

## MODELING THE DYNAMIC BEHAVIOR OF THE PARTICLE SIZE DISTRIBUTION

### 6.1 THE EXPERIMENT

A rough population balance model was proposed to describe the de-aggregation process. Flocs were formed under the same chemical conditions as in the study of the size-density relationships in Chapter 3 and introduced carefully into a baffled stirred tank, which has a volume of about 13 liters. The stirrer was then started with a rotating speed of 90 and 130 rpm for clay-$Fe^{+3}$ and clay-polymer flocs, respectively. Pictures were taken from a side window on the tank using Kodak High-Contrast Copy film and single-flash frame at successive time intervals. The film was developed with D-19 and analyzed with an Omnicon Alpha TM500 Image Analyzer (a product of Bausch & Lomb, Rochester, N.Y.) which gives the particle number concentration and size distribution of the suspension inside the tank at the selected times. The relationship between Reynolds number and mean energy dissipation for the stirred flocculator was investigated, and the result is shown in Figure 15. The Reynolds number is defined as $Re = \omega d^2/\nu$ and mean energy dissipation ($\epsilon$) is calculated from torque measurements made at various angular velocities.

### 6.2 DYNAMIC MODEL

Let:

$N(t)$ = aggregate concentration (number density)

$f(M,t)$ = function describing the distribution of particle sizes

$K_{xy}$ = breakage parameter reflecting size and strength of flocs in (x,y) interval

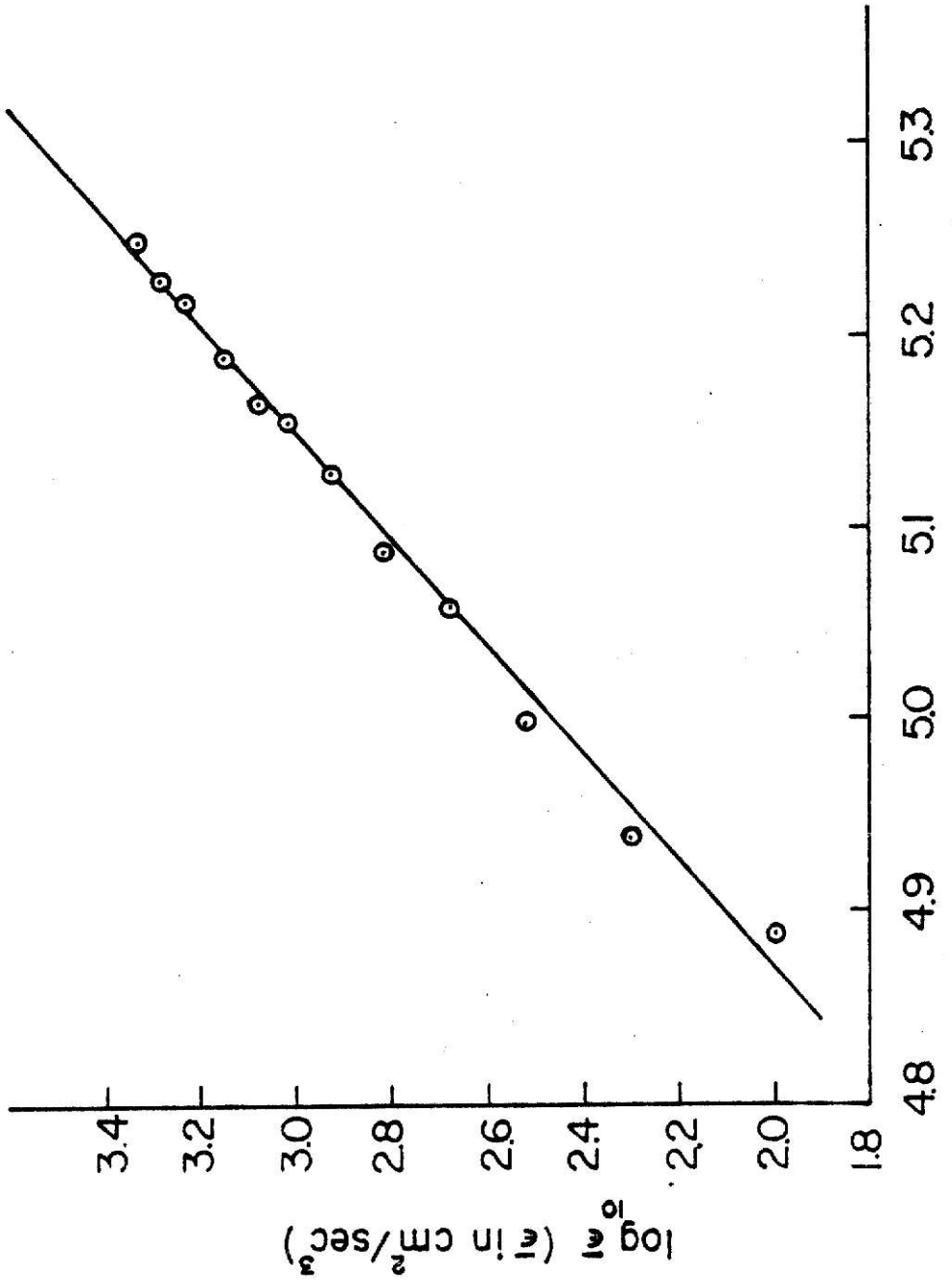


Figure 15. Relationship Between Reynolds Number and Mean Energy Dissipation.

$K_{yz}$ = breakage parameter reflecting size and strength of flocs in (y,z) interval

$t_c$ = circulation time for baffled, stirred flocculator

$\delta$ = number of daughter particles produced per fragmentation incident

g(M) = function which describes the distribution of daughter particle size (assumed to be independent of time as a simplifying approximation).

Consider the dynamic equation:

$$\frac{d}{dt}\left(N(t)\int_x^y f(M,t)dM\right) = \text{----------} \qquad (18)$$

to complete the integral population balance, the terms added to the right hand side should account for:

1) reduction in (x,y) due to breakup of interval members

2) reduction in (x,y) due to aggregation of interval members

3) increase in (x,y) due to breakup of larger particles

4) increase in (x,y) due to breakup of interval members

5) increase in (x,y) due to aggregation of smaller fragments

If the dispersion is lean or if the particular floc structure does not lend itself to reaggregation of fragments, then 2) and 5) will be negligibly small. The balance between 1) and 4) can be redressed in favor of 1) by suitable adjustment of the interval limits (x,y). Thus, a simplified population balance will appear as follows:

$$\frac{d}{dt}\left(N(t)\int_x^y f(M,t)dM\right) = -H_1(x,y) + H_3(y,z) \qquad (19)$$

Before $H_1$ and $H_3$ can be quantified, the following must be known:

i) breakage mode (average number of fragments produced per incident)

ii) distribution of fragment sizes, and

iii) breakage frequency.

6.2.1 Breakage Mode

The breakage mode for the cases under study is certainly not binary. The preliminary experiments performed upon individual floc indicate a mean for the number of fragments produced upon breakup of about 10 to 20. However, there are many more variables affecting $\delta$ than can be accounted for in simplistic population balance models (structural type and age, for example). The assumption of a particular constant value should not be regarded as indicative of the instantaneous breakup process; indeed, the selected number for $\delta$ merely represents an attempt to establish a temporal and incident-average value.

6.2.2 Distribution of Fragment Sizes:

The distribution of daughter particle sizes is very broad, ranging from colloidal size to perhaps 1500 $\mu$m. The most numerous fragments are typically 100 to 400 $\mu$m in diameter. It is likely that this rather narrow band corresponds to second or third level aggregate structures, which are more resistant to disruptive forces due to their compact conformation. It is also quite probable that primary colloidal particles are stripped from the floc surface simultaneously; the distribution of fragment sizes is possibly bimodal. For the initial purposes however, it should be sufficient to regard daughter particle size as a normal variable.

6.2.3 Breakage Frequency:

The breakage frequency will depend upon the number of metastable flocs present in the system and certain rate-determining variables pertinent to the deaggregation mechanism. Experimental evidence gathered thus far suggests that the principal mechanism responsible for aggregate size reduction in a baffled, stirred flocculator is interaction with the impeller

stream and vortex system. The observed large-scale fragmentation probably takes place in the impeller stream in the vicinity of the blade tips. According to Holmes, Voncken, and Dekker (1964) a circulation time can be defined as the residence time in a loop, averaged over all streamlines. For a given $Re_{imp}$, Holmes et al. give:

$$t_c = \frac{0.85\ D^2}{d^2} \tag{20}$$

For the apparatus used here, D = 31 cm, d = 7.65 cm, and $\omega$ = 9.6 rad/sec for clay-$Fe^{+3}$ floc and 13.7 rad/sec for clay-polymer floc. The $Re_{imp}$ were calculated to be 55,930 and 79,946 respectively, and thus $t_c$ = 1.45 and 1.02 seconds.

The inverse of the circulation time can be thought of as an indicator of the frequency at which flocs encounter the impeller stream. A very simple model, therefore would express the breakage frequency, $f_b$, for flocs of a particular size and structural type as:

$$f_b = K \,/\, t_c \tag{21}$$

where the dimensionless parameter K will reflect floc size, type, and strength. A highly simplified integral population balance model can now be written:

$$\frac{d}{dt}\left(N(t)\int_x^y f(M,t)dM\right) = -\frac{Kxy}{t_c} N(t)\int_x^y f(M,t)dM + \frac{Kyz}{t_c}\delta N(t)\int_y^z f(M,t)dM\int_x^y g(M)dM \tag{22}$$

## 6.3 DATA TREATMENT

According to Smith and Jordan (1964) the log-normal law serves as an excellent mathematical model for many small particle size distributions.

The experimental number and size distribution data obtained were therefore plotted on log-probability paper; a straight line indicates good agreement with the log-normal distribution. An example of such a plot is shown in Figure 16. It should be noted that the fit is not good for very small t's. Mean floc size and standard deviation are found from the plots for each time period. The function f(M,t) is defined completely since according to the definition of log-normal function:

$$y' = \frac{1}{\ln \sigma_g \sqrt{2\pi}} \exp\left(-\frac{(\ln X - \ln \bar{M})^2}{2(\ln \sigma_g)^2}\right) \qquad (23)$$

where y' is the probability density function.

N(t) can be found directly from analysis of the developed film. The left hand side of equation (29) can now be calculated; some results are shown in Table 4. The size interval (x,y) chosen here is (600 - 800 $\mu$m).

In order to evaluate the right hand side of equation (29) the mean and standard deviation of the daughter particle size distribution (assumed normal), a functional relationship between number of daughter particle produced by fragmentation under various physical conditions, and an appropriate size interval (y,z), have to be found first. Unfortunately, the information at hand so far is not sufficient to permit detailed use of the population balance model. As an illustration of the possibilities, however, sample values of the necessary parameters were inserted into equation (29) and the results (Table 4) compared with a typical deaggregation experiment. The size interval (y,z) chosen here is (800 - 1200 $\mu$m). The assumed values of the mean and standard deviation of the daughter particle size distribution are 430 $\mu$m and 120 $\mu$m, respectively; $\delta$ is assumed to be equal to 10 since this is typical of the values observed. $K_{xy}$, $K_{yz}$ are chosen as 0.004

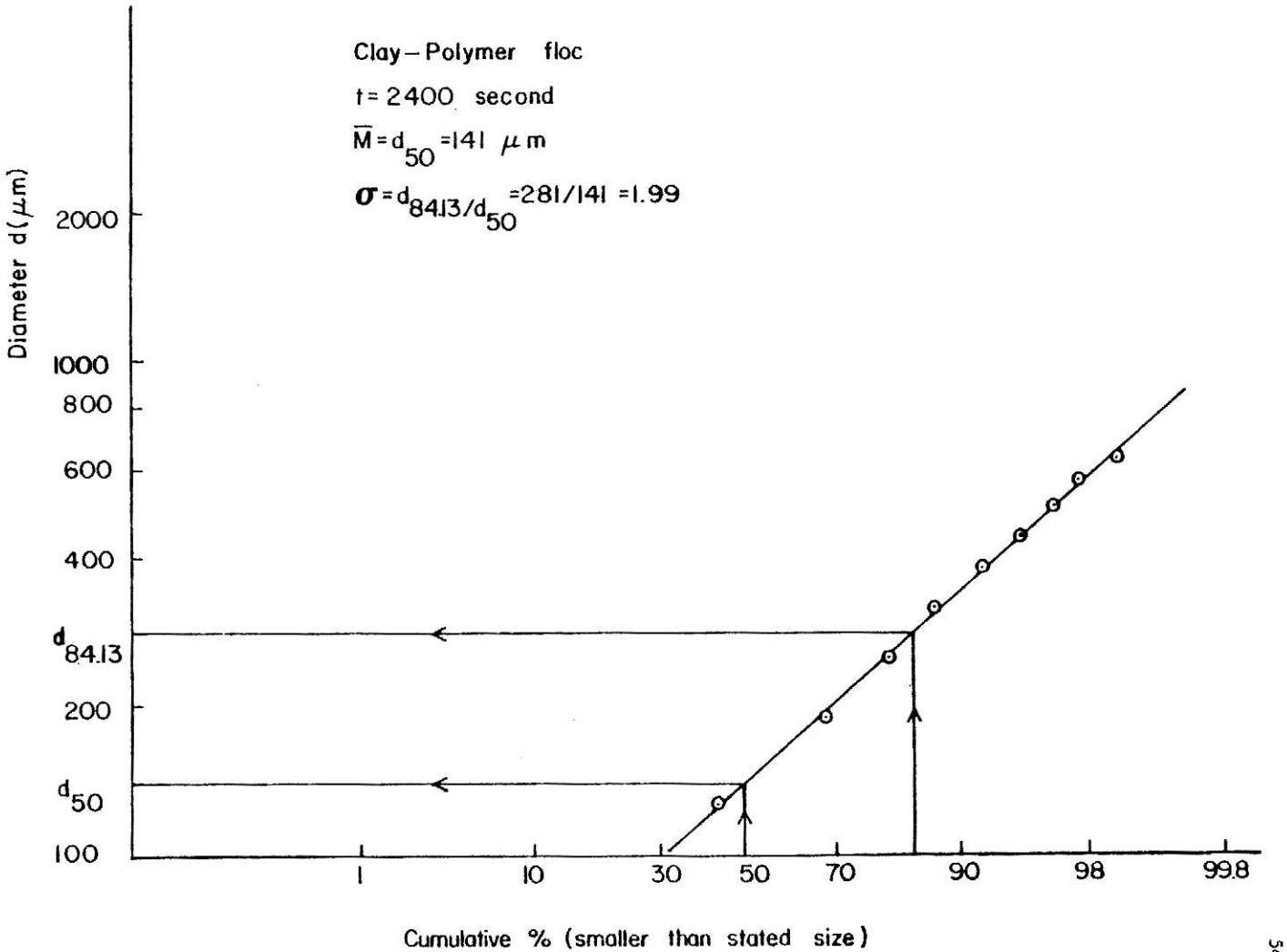


Figure 16. Log-Normal Distribution.

TABLE 4

COMPARISON OF THEORETICAL AND EXPERIMENTAL VALUE OF POPULATION BALANCE MODEL (CLAY-$Fe(OH)_3$ FLOC)

| Time (second) | Predicted x $10^3$ | Experimental x $10^3$ |
|---|---|---|
| 15 | 38.01 | 39.60 |
| 180 | 4.79 | 2.74 |
| 360 | 1.86 | 2.62 |
| 600 | 1.17 | 1.36 |
| 1800 | 0.12 | 0.10 |

and 0.0096 respectively. Table 4 shows qualitative agreement between experimental results and computed values. The quality of fit depends on the choice of parameters, of course.

An attractive variation of integral population balance technique is the model presented by Ramkrishna (1974) employing the cumulative volume distribution function (F) instead of the number distribution cited earlier. For a batch vessel when the dispersion is lean in the dispersed phase Ramkrishna gives:

$$\partial F/\partial t = \int_v^\infty \Gamma(v')G(v,v')dF(v',t) \qquad (24)$$

where G is cumulative distribution function of daughter droplet size arising from breakage of a larger droplet in terms of volume fraction. Ramkrishna assumes the breakage frequency function $\Gamma(v)$ can be formulated as:

$$\Gamma(v) = Cv^n \qquad (25)$$

where C and n are constants. In an effort to solve equation (24) a similarity variable $z = (1+Ct)v^n$ has been used. For a fixed value of F(v,t) the similarity variable z is constant and for t sufficiently large:

$$v^n = \text{constant}$$

Thus a log-log plot of v vs. t should produce a straight line with negative slope of -1/n. Further, similar plots for different fixed values of F(v,t) should yield a set of parallel straight lines. For a study of clay-$Fe^{+3}$ flocs such a plot is shown in Figure 18. The slope of straight lines in Figure 18 show an average value of $n \sim 6.38$, i.e., $\Gamma(v) \sim d^{6.38}$. The breakage function should reflect the relationship between floc strength and the effective energy for floc breakup. Valentas, Bilous, and Amundson (1966) state that there is no evidence for assuming a size dependence

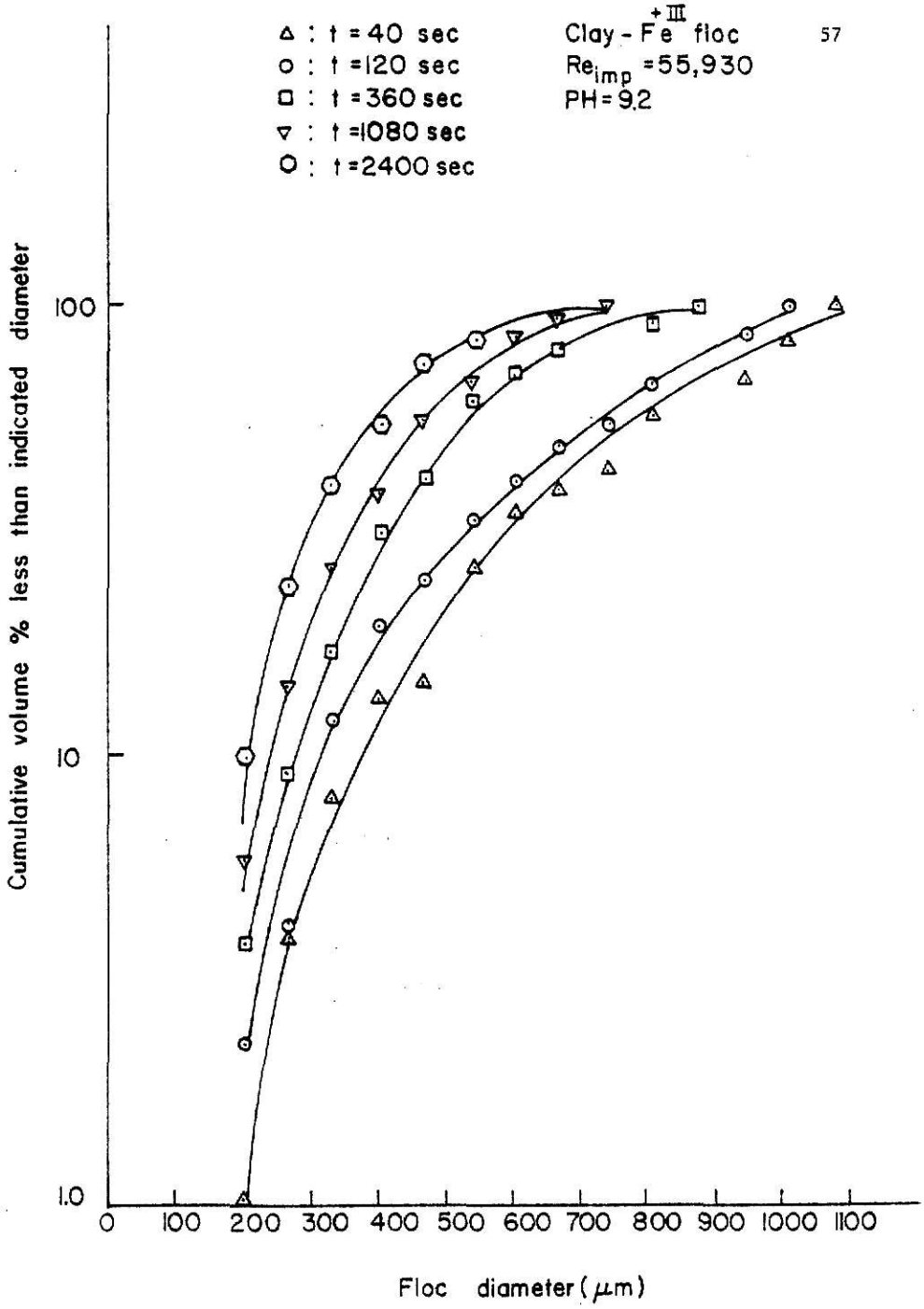


Figure 17. Cumulative Volume Distribution.

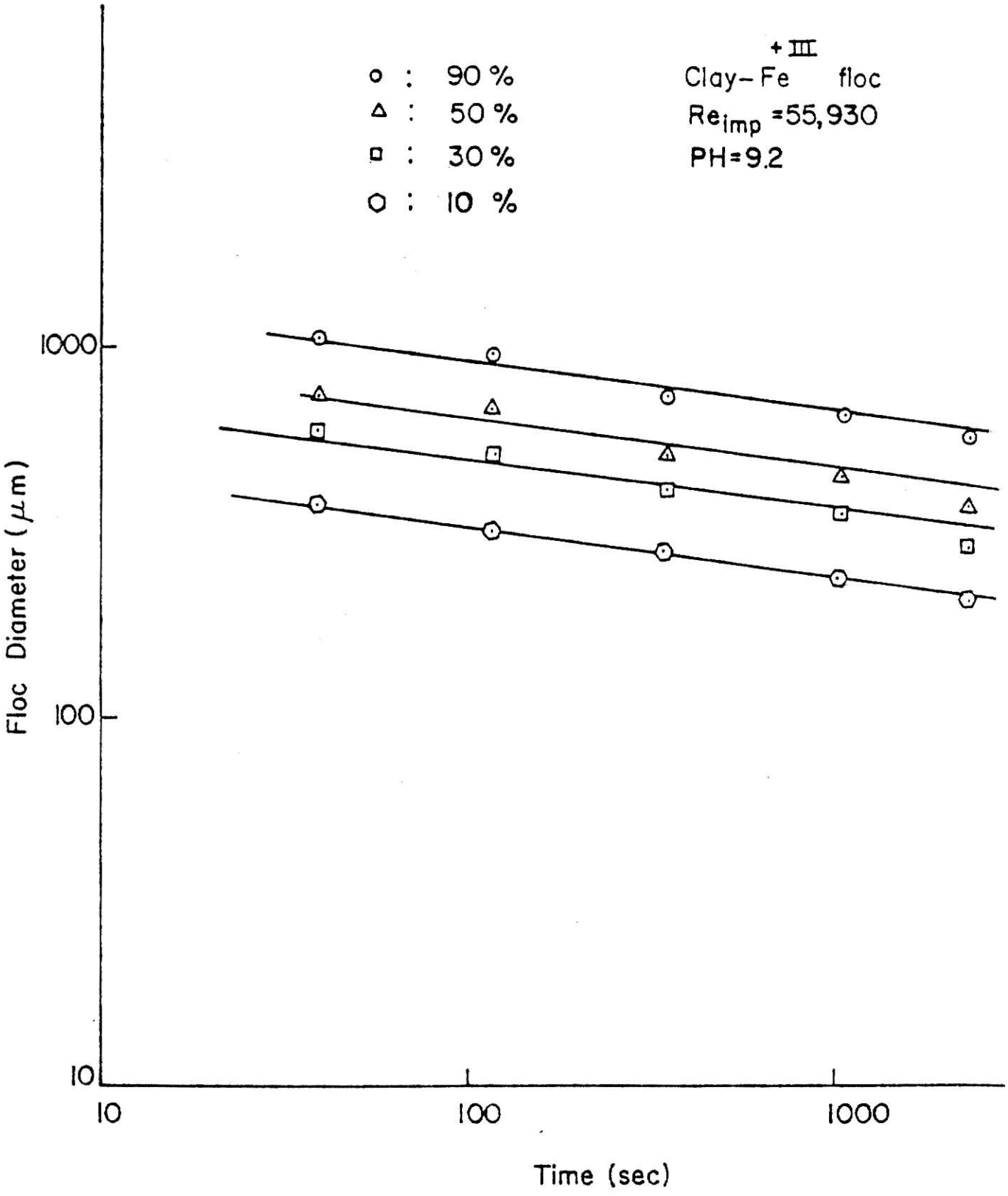
+ III
o : 90 %
Δ : 50 %
□ : 30 %
○ : 10 %
Clay–Fe floc
Re_imp =55,930
PH=9.2
1000
100
10
Floc Diameter (μm)
10
100
1000
Time (sec)

Figure 18.

greater than $d^3$ on the breakage frequency. Such a high order dependency of $\Gamma(v)$ on floc diameter may be due to the extremely abnormal distribution of energy dissipation inside the tank. In addition, there is no direct information regarding the relative magnitudes of C and t so the choice of a sufficiently large t is still open to question.

NOTATION

| | | |
|---|---|---|
| $C$ | Breakage frequency constant | |
| $f$ | Diameter of impeller | cm |
| $D$ | Diameter of tank | cm |
| $f_b$ | As defined in the text | |
| $f(M,t)$ | As defined in the text | |
| $F(v,t)$ | As defined in the text | |
| $g(M)$ | As defined in the text | |
| $G$ | As defined in the text | |
| $K$ | As defined in the text | |
| $K_{xy}$, $K_{yz}$ | As defined in the text | |
| $\bar{M}$ | Mean of log-normal function | mm |
| $N(t)$ | As defined in the text | |
| $t_c$ | As defined in the text | |
| $v,v'$ | Volume of floc | $mm^3$ |
| $X$ | Size of floc | mm |
| $y'$ | Probability density variable | |
| $z$ | Similarity variable | |

GREET LETTERS

| | | |
|---|---|---|
| $\delta$ | Number of daughter particles produced by breakage | |
| $\sigma_g$ | Standard deviation of log-normal function | |
| $\nu$ | Kinematic viscosity | $cm^2/sec^3$ |
| $\omega$ | Angular velocity | rad/sec |
| $\Gamma(v)$ | Breakage frequency function | |

## REFERENCE

1. Holmes, D. B., Voncken, R. M., & Dekker, J A., "Fluid flow in turbulent-stirred, baffled tanks-I," Chem. Engng. Sci., 19, 201 (1964).

2. Valentas, K. J., Bilous, O., & Amundson, A. R., "Analysis of breakage in dispersed phase systems," I & EC Fundamentals, 5,271 (1966).

3. Ramkrishna, D., "Drop-breakage in agitated liquid-liquid dispersions," Chem. Engr. Sci., 29, 987 (1974).

4. Smith J. E. & Jordan, M. L , "Mathematical and graphical interpretation of the log-normal law for particle size distribution," J. Colloid Sci., 19, 549 (1964).

# CHAPTER 7

## CONCLUSIONS

This study has shown that aggregate breakup in a turbulent jet at moderate Reynolds number occurs in response to stresses imposed by the mean flow or by integral scale eddies; the daughter particles produced are relatively large and the reduction of the parent aggregate occurs by fragmentation, not by primary particle erosion. Selection of a turbulent jet for investigation of aggregate breakup is particularly appropriate, for it provides an environment similar to that experienced by flocs when they encounter the impeller stream in a baffled, stirred flocculator. The local dissipation rate, $\epsilon$, required for fragmentation of large kaolin-$Fe(OH)_3$ and kaolin-polymer flocs was found to be on the order of 1000 to 2000 $cm^2/sec^3$. In general, higher dissipation rates produced larger number of fragments, probably due to increased energy availability at larger wave number. This high Reynolds number behavior may be somewhat similar to the comminution mechanism suggested by Ali et al. (1979) in their study of the dispersion of oil in water in agitated vessels, although in the present case, high frequency interactions between the floc structure and small-scale fluid motions could not be detected. In all of the photographic evidence obtained in this study of floc breakup, the daughter particles appear to be more compact structures, characteristic of a lower level of aggregation.

A principle advantage of the experimental method employed in this work is that it permitted quantitative estimates of floc strength to be made. Earlier studies of floc strength, for example, Hannah, Cohen, and Robeck (1967), depended upon indirect measurements to produce qualitative assessments of floc strength; Hannah et al. measured the size distribution of

fragments produced when the parent aggregate was forced through a 70 $\mu$m orifice. In contrast, for the investigation made here, the strength of floc could be deduced directly from the photographic record. For kaolin-$Fe^{+3}$ flocs, it is found that a pH of 9.5 produced aggregates that were about 75 percent stronger than those formed at a pH of 7.4. It seems evident that this difference is the result of a more rapid and complete hydrolysis (formation of $Fe(OH)_3$ at the elevated pH). For kaolin-polymer flocs, the difference in strength between those formed at pH 7.2 and pH 10.6 is due to the conformational difference of the polyelectrolyte, with those formed at elevated pH being very marginally stronger. It is particularly interesting to note that the regression lines yield a strength expression proportional to $\bar{d}^{2.4}$; the critical force requirement per unit mass is not constant, reinforcing the thought that structural differences exist as a function of size.

Confirmation of the multiple-level hypothesis was obtained by measuring floc densities and recording these data as a function of floc size. For kaolin-$Fe(OH)_3$ flocs formed at a pH of 9.5, there was a pronounced increase in apparent density for decreasing floc size beginning at about $\bar{d}$ = 2 mm. If all flocs were built up by the addition of sub-units of a given size and set fraction of immobilized water, then the size-density data could not possible exhibit this type of relationship. More importantly, deaggregation could not occur by the large-scale fragmentation process shown to exist by this investigation.

The batch deaggregation experiments performed indicated the log-normal function can adequately describe the floc size distributions at

advanced t's. Although quantitative results are not complete for evaluating the parameters of the dynamic model, some conclusions can be inferred from the study. For example, breakage parameters $K_{xy}$ and $K_{yz}$ should reflect the strength of flocs within the sizes indicated so the ratio $K_{xy}/K_{yz}$ should be proportional to $S_{yz}/S_{xy}$ to some extent. Besides, if different structural types do exist among flocs of comparable sizes, $K_{xy}$ and $K_{yz}$ would show a time dependence since in general, weaker flocs of a given size suffer breakage earlier than the stronger ones.

A future study should examine the daughter particle size distribution and number produced as a function of various physical parameters; it is strongly recommended that a more complete dynamic model be formulated and refined with additional data.

ACKNOWLEDGMENT

The author wishes to express his thanks to Dr. L. A Glasgow for his direction and steady encouragement throughout this study. Thanks are also due to Dr. L. T. Fan and Dr. J. K. Koilleker for their suggestions and discussions.

The financial support for this investigation was provided by the National Science Foundation under Grant No. ENG-7908093. This support is gratefully acknowledged.

# APPENDIX

List of computer programs:

1. Numerical integration of the population balance model.
2. Estimation the parameters of the population balance model.

```
    $JOB
1       COMMON A2,A3,A4,A5,SIGMA1,XMEAN,T
C       NUMERICAL INTEGRATION OF POPULATION BALANCE MODEL (EQ.(29)).
C       THE SIXTH NEWTON-COTES FORMULA WAS USED.
C       W(M,T) = DIFFERENTIATE OF F(M,T) WITH RESPECT TO TIME.
C       T = TIME
C       XN = N(T) = NUMBER OF FLOCS AT TIME T.
C       XMEAN = MEAN FLOC DIAMETER AT TIME T.
C       KAOLIN-FE FLOCS, PH = 9.2
2      10 FORMAT(5X,F8.2,4X,E11.3,7X,E11.3)
3      11 FORMAT(F6.1)
4      12 FORMAT(//5X,F7.1,5X,F6.1,9X,F7.1)
5      13 FORMAT(///'      TIME(SEC)    MEAN SIZE(MEU)    NO. OF FLOC')
6      90 FORMAT(///5X,'SIZE(MEU)  INTEGRAN F(M,T)  INTEGRAN W(M,T)')
7          A2=247.865
8          A3=-13.767
9          SIGMA1=2.19
10         A6=34.47
11         A7=0.30891
12         A4=SQRT(2.)*ALOG(SIGMA1)
13         A5=SQRT(3.141593)*A4
14         READ(5,11) T
15         WRITE(6,13)
16         XMEAN=A2+A3*ALOG(T)
17         XN=A6*T**A7
18         WRITE(6,12) T,XMEAN,XN
19         WRITE(6,90)
20         XO=10.
21         X1=10.
22         FX=0.
23         WX=0.
24      1  CONTINUE
25         XO0=ALOG(XO)
26         X11=ALOG(X1)
27         H1=(X11-XO0)/6.
28         CALL F(XO,Y01,Y03)
29         Z11=XO0+H1
30         CALL F(Z11,Y11,Y13)
31         Z22=Z11+H1
32         CALL F(Z22,Y21,Y23)
33         Z33=Z22+H1
34         CALL F(Z33,Y31,Y33)
35         Z44=Z33+H1
36         CALL F(Z44,Y41,Y43)
37         Z55=Z44+H1
38         CALL F(Z55,Y51,Y53)
39         Z66=Z55+H1
40         CALL F(Z66,Y61,Y63)
41         FX=3.*H1*(Y01+5.*Y11+Y21+6.*Y31+Y41+5.*Y51+Y61)/10.+FX
42         WX=3.*H1*(Y03+5.*Y13+Y23+6.*Y33+Y43+5.*Y53+Y63)/10.+WX
43         WRITE(6,10) X1,FX,WX
44         XO=X1
45         X1=X1+10.
46         IF(X1.GT.2000.) GO TO 100
47         GO TO 1
48     100 CONTINUE
49         STOP
50         END

51         SUBROUTINE F(ZF,YF,YW)
```

```
52          COMMON A2,A3,A4,A5,SIGMA1,XMEAN,T
53          ZZF=((ZF-ALOG(XMEAN))/A4)**2
54          IF(ZZF.GT.25.)  GO TO 111
55          YF=EXP(-ZZF)/A5
56          YW=2.*YF*A3*(ZF-ALOG(XMEAN))/A4/A4/T/XMEAN
57          GO TO 112
58      111 CONTINUE
59          YF=0.
60          YW=0.
61      112 CONTINUE
62          RETURN
63          END
```

```
     $ENTRY
```

| TIME(SEC) | MEAN SIZE(MEU) | NO. OF FLOC |
|---|---|---|
| 3600.0 | 135.1 | 432.5 |

| SIZE(MEU) | INTEGRAN F(M,T) | INTEGRAN W(M,T) |
|---|---|---|
| 10.00 | 0.0000E 00 | 0.0000E 00 |
| 20.00 | 0.695E-02 | 0.681E-06 |
| 30.00 | 0.27CE-01 | 0.222E-05 |
| 40.00 | 0.598E-01 | 0.42?E-05 |
| 50.00 | 0.102E 00 | 0.63?E-05 |
| 60.00 | 0.15CE 00 | 0.837E-05 |
| 70.00 | 0.2CCE 00 | 0.1C1E-04 |
| 80.00 | 0.251E 00 | 0.115E-04 |
| 90.00 | 0.302E 00 | 0.125E-04 |
| 100.00 | 0.35CE 00 | 0.132E-04 |
| 110.00 | 0.396E 00 | 0.135E-04 |
| 120.00 | 0.439E 00 | 0.142E-04 |
| 130.00 | 0.48CE 00 | 0.143E-04 |
| 140.00 | 0.518E 00 | 0.143E-04 |
| 150.00 | 0.553E 00 | 0.142E-04 |
| 160.00 | 0.585E 00 | 0.14CE-04 |
| 170.00 | 0.615E 00 | 0.137E-04 |
| 180.00 | 0.642E 00 | 0.134E-04 |
| 190.00 | 0.668E 00 | 0.130E-04 |
| 200.00 | 0.691E 00 | 0.127E-04 |
| 210.00 | 0.713E 00 | 0.122E-04 |
| 220.00 | 0.732E 00 | 0.118E-04 |
| 230.00 | 0.751E 00 | 0.114E-04 |
| 240.00 | 0.768E 00 | 0.11CE-04 |
| 250.00 | 0.783E 00 | 0.1C5E-04 |
| 260.00 | 0.798E 00 | 0.1C1E-04 |
| 270.00 | 0.811E 00 | 0.969E-05 |
| 280.00 | 0.823E 00 | 0.929E-05 |
| 290.00 | 0.835E 00 | 0.89CE-05 |
| 300.00 | 0.845E 00 | 0.853E-05 |
| 310.00 | 0.855E 00 | 0.816E-05 |
| 320.00 | 0.864E 00 | 0.781E-05 |
| 330.00 | 0.872E 00 | 0.747E-05 |
| 340.00 | 0.88CE 00 | 0.715E-05 |
| 350.00 | 0.887E 00 | 0.683E-05 |

| | | |
|---|---|---|
| 360.00 | 0.894E 00 | 0.654E-05 |
| 370.00 | 0.900E 00 | 0.625E-05 |
| 380.00 | 0.906E 00 | 0.598E-05 |
| 390.00 | 0.911E 00 | 0.572E-05 |
| 400.00 | 0.916E 00 | 0.547E-05 |
| 410.00 | 0.921E 00 | 0.523E-05 |
| 420.00 | 0.926E 00 | 0.500E-05 |
| 430.00 | 0.930E 00 | 0.478E-05 |
| 440.00 | 0.934E 00 | 0.458E-05 |
| 450.00 | 0.937E 00 | 0.438E-05 |
| 460.00 | 0.940E 00 | 0.419E-05 |
| 470.00 | 0.944E 00 | 0.401E-05 |
| 480.00 | 0.947E 00 | 0.384E-05 |
| 490.00 | 0.949E 00 | 0.368E-05 |
| 500.00 | 0.952E 00 | 0.352E-05 |
| 510.00 | 0.954E 00 | 0.337E-05 |
| 520.00 | 0.957E 00 | 0.323E-05 |
| 530.00 | 0.959E 00 | 0.309E-05 |
| 540.00 | 0.961E 00 | 0.296E-05 |
| 550.00 | 0.963E 00 | 0.284E-05 |
| 560.00 | 0.965E 00 | 0.272E-05 |
| 570.00 | 0.966E 00 | 0.261E-05 |
| 580.00 | 0.968E 00 | 0.250E-05 |
| 590.00 | 0.970E 00 | 0.240E-05 |
| 600.00 | 0.971E 00 | 0.230E-05 |
| 610.00 | 0.972E 00 | 0.221E-05 |
| 620.00 | 0.974E 00 | 0.212E-05 |
| 630.00 | 0.975E 00 | 0.204E-05 |
| 640.00 | 0.976E 00 | 0.195E-05 |
| 650.00 | 0.977E 00 | 0.188E-05 |
| 660.00 | 0.978E 00 | 0.180E-05 |
| 670.00 | 0.979E 00 | 0.173E-05 |
| 680.00 | 0.980E 00 | 0.166E-05 |
| 690.00 | 0.981E 00 | 0.160E-05 |
| 700.00 | 0.982E 00 | 0.154E-05 |
| 710.00 | 0.982E 00 | 0.148E-05 |
| 720.00 | 0.983E 00 | 0.142E-05 |
| 730.00 | 0.984E 00 | 0.136E-05 |
| 740.00 | 0.985E 00 | 0.131E-05 |
| 750.00 | 0.985E 00 | 0.126E-05 |
| 760.00 | 0.986E 00 | 0.121E-05 |
| 770.00 | 0.986E 00 | 0.117E-05 |
| 780.00 | 0.987E 00 | 0.112E-05 |
| 790.00 | 0.987E 00 | 0.108E-05 |
| 800.00 | 0.988E 00 | 0.104E-05 |
| 810.00 | 0.988E 00 | 0.100E-05 |
| 820.00 | 0.989E 00 | 0.964E-06 |
| 830.00 | 0.989E 00 | 0.929E-06 |
| 840.00 | 0.990E 00 | 0.894E-06 |
| 850.00 | 0.990E 00 | 0.861E-06 |
| 860.00 | 0.990E 00 | 0.829E-06 |
| 870.00 | 0.991E 00 | 0.799E-06 |
| 880.00 | 0.991E 00 | 0.770E-06 |
| 890.00 | 0.991E 00 | 0.742E-06 |
| 900.00 | 0.992E 00 | 0.715E-06 |
| 910.00 | 0.992E 00 | 0.689E-06 |
| 920.00 | 0.992E 00 | 0.664E-06 |
| 930.00 | 0.993E 00 | 0.640E-06 |
| 940.00 | 0.993E 00 | 0.617E-06 |
| 950.00 | 0.993E 00 | 0.594E-06 |

| | | |
|---|---|---|
| 960.00 | 0.993E 00 | 0.573E-06 |
| 970.00 | 0.994E 00 | 0.552E-06 |
| 980.00 | 0.994E 00 | 0.533E-06 |
| 990.00 | 0.994E 00 | 0.514E-06 |
| 1000.00 | 0.994E 00 | 0.495E-06 |
| 1010.00 | 0.994E 00 | 0.477E-06 |
| 1020.00 | 0.995E 00 | 0.460E-06 |
| 1030.00 | 0.995E 00 | 0.444E-06 |
| 1040.00 | 0.995E 00 | 0.428E-06 |
| 1050.00 | 0.995E 00 | 0.413E-06 |
| 1060.00 | 0.995E 00 | 0.398E-06 |
| 1070.00 | 0.995E 00 | 0.384E-06 |
| 1080.00 | 0.996E 00 | 0.370E-06 |
| 1090.00 | 0.996E 00 | 0.357E-06 |
| 1100.00 | 0.996E 00 | 0.345E-06 |
| 1110.00 | 0.996E 00 | 0.332E-06 |
| 1120.00 | 0.996E 00 | 0.320E-06 |
| 1130.00 | 0.996E 00 | 0.309E-06 |
| 1140.00 | 0.996E 00 | 0.298E-06 |
| 1150.00 | 0.996E 00 | 0.287E-06 |
| 1160.00 | 0.997E 00 | 0.277E-06 |
| 1170.00 | 0.997E 00 | 0.267E-06 |
| 1180.00 | 0.997E 00 | 0.258E-06 |
| 1190.00 | 0.997E 00 | 0.248E-06 |
| 1200.00 | 0.997E 00 | 0.239E-06 |
| 1210.00 | 0.997E 00 | 0.231E-06 |
| 1220.00 | 0.997E 00 | 0.222E-06 |
| 1230.00 | 0.997E 00 | 0.214E-06 |
| 1240.00 | 0.997E 00 | 0.206E-06 |
| 1250.00 | 0.997E 00 | 0.199E-06 |
| 1260.00 | 0.997E 00 | 0.192E-06 |
| 1270.00 | 0.997E 00 | 0.184E-06 |
| 1280.00 | 0.997E 00 | 0.178E-06 |
| 1290.00 | 0.998E 00 | 0.171E-06 |
| 1300.00 | 0.998E 00 | 0.165E-06 |
| 1310.00 | 0.998E 00 | 0.158E-06 |
| 1320.00 | 0.998E 00 | 0.152E-06 |
| 1330.00 | 0.998E 00 | 0.147E-06 |
| 1340.00 | 0.998E 00 | 0.141E-06 |
| 1350.00 | 0.998E 00 | 0.135E-06 |
| 1360.00 | 0.998E 00 | 0.130E-06 |
| 1370.00 | 0.998E 00 | 0.125E-06 |
| 1380.00 | 0.998E 00 | 0.120E-06 |
| 1390.00 | 0.998E 00 | 0.115E-06 |
| 1400.00 | 0.998E 00 | 0.111E-06 |
| 1410.00 | 0.998E 00 | 0.106E-06 |
| 1420.00 | 0.998E 00 | 0.102E-06 |
| 1430.00 | 0.998E 00 | 0.975E-07 |
| 1440.00 | 0.998E 00 | 0.934E-07 |
| 1450.00 | 0.998E 00 | 0.894E-07 |
| 1460.00 | 0.998E 00 | 0.855E-07 |
| 1470.00 | 0.998E 00 | 0.818E-07 |
| 1480.00 | 0.998E 00 | 0.782E-07 |
| 1490.00 | 0.998E 00 | 0.746E-07 |
| 1500.00 | 0.998E 00 | 0.712E-07 |
| 1510.00 | 0.999E 00 | 0.679E-07 |
| 1520.00 | 0.999E 00 | 0.647E-07 |
| 1530.00 | 0.999E 00 | 0.615E-07 |
| 1540.00 | 0.999E 00 | 0.585E-07 |
| 1550.00 | 0.999E 00 | 0.555E-07 |

```
1560.00       0.999E 00          0.527E-07
1570.00       0.999E 00          0.499E-07
1580.00       0.999E 00          0.472E-07
1590.00       0.999E 00          0.446E-07
1600.00       0.999E 00          0.422E-07
1610.00       0.999E 00          0.399E-07
1620.00       0.999E 00          0.377E-07
1630.00       0.999E 00          0.356E-07
1640.00       0.999E 00          0.335E-07
1650.00       0.999E 00          0.317E-07
1660.00       0.999E 00          0.299E-07
1670.00       0.999E 00          0.282E-07
1680.00       0.999E 00          0.266E-07
1690.00       0.999E 00          0.251E-07
1700.00       0.999E 00          0.237E-07
1710.00       0.999E 00          0.223E-07
1720.00       0.999E 00          0.211E-07
1730.00       0.999E 00          0.199E-07
1740.00       0.999E 00          0.188E-07
1750.00       0.999E 00          0.177E-07
1760.00       0.999E 00          0.167E-07
1770.00       0.999E 00          0.158E-07
1780.00       0.999E 00          0.149E-07
1790.00       0.999E 00          0.141E-07
1800.00       0.999E 00          0.133E-07
1810.00       0.999E 00          0.125E-07
1820.00       0.999E 00          0.118E-07
1830.00       0.999E 00          0.111E-07
1840.00       0.999E 00          0.105E-07
1850.00       0.999E 00          0.992E-08
1860.00       0.999E 00          0.935E-08
1870.00       0.999E 00          0.882E-08
1880.00       0.999E 00          0.832E-08
1890.00       0.999E 00          0.785E-08
1900.00       0.999E 00          0.740E-08
1910.00       0.999E 00          0.698E-08
1920.00       0.999E 00          0.659E-08
1930.00       0.999E 00          0.621E-08
1940.00       0.999E 00          0.586E-08
1950.00       0.999E 00          0.553E-08
1960.00       0.999E 00          0.521E-08
1970.00       0.999E 00          0.492E-08
1980.00       0.999E 00          0.464E-08
1990.00       0.999E 00          0.438E-08
2000.00       0.999E 00          0.413E-08

CORE USAGE       OBJECT CODE=     2896 BYTES,ARRAY AREA=       28 BYTES,TOTAL AREA AVAILAB
DIAGNOSTICS       NUMBER OF ERRORS=        0, NUMBER OF WARNINGS=        0, NUMBER OF EXT
COMPILE TIME=     0.20 SEC,EXECUTION TIME=     1.78 SEC,     22.30.33    WEDNESDAY    29
```

```
      $JOB
1           DIMENSION A(50),B(50),C(50)
C       THIS PROGRAM IS USED TO SOLVE THE PARAMETERS KXY,KYZ IN POPULATION
C         BALANCE MODEL
C         KAGLIN-FEELOC
C         N = NUMBER OF SIMULTANEOUS EQUATIONS OF THE FORM
C         A(I)*KXY+B(I)*KYZ = C(I)
C         A(I) = 1ST TERM OF R.H.S. OF EQ.(29) EXCLUDING KXY.
C         B(I) = 2ND TERM OF R.H.S. OF EQ.(29) EXCLUDING KYZ.
C         C(I) = L.H.S. OF EQ.(29).
C         I = 1, T = 15 SECOND
C         I = 2,T = 180 SECOND
C         I = 3, T = 360 SECOND
C         I = 4, T = 600 SECOND
C         I = 5, T = 1800 SECOND
 2          1 FORMAT(I2)
 3          2 FORMAT(F8.4,3X,F8.4,3X,E11.4)
 4          3 FORMAT(///5X,'VALUE OF N')
 5          4 FORMAT(/8X,I3)
 6          5 FORMAT(//9X,'KXY',10X,'KYZ',10X,'RATIO',5X,'PAIR')
 7          8 FORMAT(/4X,F10.7,4X,F10.7,4X,F8.3,3X,I3,I3)
 8         11 FORMAT(///7X,'A(I)        B(I)          C(I)')
 9         21 FORMAT(/4X,F8.4,3X,F8.4,3X,E11.4)
10            READ(5,1) N
11            WRITE(6,3)
12            WRITE(6,4) N
13            DO 90 I=1,N
14            READ(5,2) A(I),B(I),C(I)
15         90 CONTINUE
16            WRITE(6,11)
17            DO 12 I=1,N
18            WRITE(6,21) A(I),B(I),C(I)
19         12 CONTINUE
20            WRITE(6,5)
21            J=N-1
22            DO 6 K=1,J
23            M=K+1
24            DO 7 L=M,N
25            XKXY=(C(K)*B(L)-C(L)*B(K))/(A(K)*B(L)-A(L)*B(K))
26            XKYZ=(A(K)*C(L)-A(L)*C(K))/(A(K)*B(L)-A(L)*B(K))
27            RATIO=XKYZ/XKXY
28            WRITE(6,8) XKXY,XKYZ,RATIO,K,L
29          7 CONTINUE
30          6 CONTINUE
31            STOP
32            END
      $ENTRY


VALUE OF N
      5


  A(I)        B(I)           C(I)
-4.7940      6.1241      0.3801E-01
```

```
   -4.8960      2.3256     0.4787E-02
   -6.1040      2.8166     0.1865E-02
   -6.5260      2.8614     0.1168E-02
   -8.0200      3.3524     0.1177E-03

      KXY          KYZ          RATIO      PAIR
   0.0031368    0.0086621      2.761       1  2
   0.0040051    0.0093419      2.332       1  3
   0.0038711    0.0092369      2.386       1  4
   0.0038344    0.0092082      2.401       1  5
   0.0225607    0.0495546      2.197       2  3
   0.0094061    0.0218608      2.324       2  4
   0.0070485    0.0168973      2.397       2  5
   0.0022365    0.0055090      2.463       3  4
   0.0027848    0.0066972      2.405       3  5
   0.0033426    0.0080316      2.403       4  5
CORE USAGE     OBJECT CODE=    1688 BYTES,ARRAY AREA=     600 BYTES,TOTAL AREA A
DIAGNOSTICS      NUMBER OF ERRORS=       0, NUMBER OF WARNINGS=       0, NUMBER
COMPILE TIME=     0.13 SEC,EXECUTION TIME=     0.08 SEC,     22.30.34    WEDNESDAY
```

# THE BREAKUP OF FLOCS IN A TURBULENT FLOW FIELD

by

JYH PING HSU

B. S., National Taiwan University, 1977

---

AN ABSTRACT OF A MASTER'S THESIS

submitted in partial fulfillment of the

requirements for the degree

MASTER OF SCIENCE

Department of Chemical Engineering

KANSAS STATE UNIVERSITY
Manhattan, Kansas

1980

Photographic observation of floc disintegration resulting from interaction with a horizontally-directed turbulent jet reveals a large-scale fragmentation mechanism; the breakup occurs in response to stresses imposed by the mean flow or integral-scale eddies. In addition to the visualization of aggregate breakup, the experimental method permitted quantitative determination of floc strength. Flocs formed by the aggregation of colloidal kaolin with a high-molecular weight polyacrylamide were found to be more than twice as strong as kaolin-$Fe(OH)_3$ flocs of the same size. Examination of floc density and strength at different levels of pH reveals that the conformation of polymer largely determined the structural type and thus the strength of flocs. The number and size of daughter particles produced upon fragmentation varied widely, with higher local dissipation rates, in general, producing more fragments. The evidence gathered in this study suggests that the daughter particles are sub-units, lower-level structures of a more compact conformation that when loosely affiliated, form the parent floc. A population balance model was proposed to describe the deaggregation history of flocs inside a baffled, stirred tank. Preliminary data obtained shows that the log-normal distribution function adequately describes the size distribution of the flocs. Using the similarity variable suggested by Ramkrishna (1974), the breakage frequency was found to be proportional to floc diameter to sixth power.